

This discussion paper is/has been under review for the journal Atmospheric Chemistry and Physics (ACP). Please refer to the corresponding final paper in ACP if available.

Aerosol microphysics simulations of the Mt. Pinatubo eruption with the UKCA composition-climate model

S. S. Dhomse¹, K. M. Emmerson², G. W. Mann^{1,3}, N. Bellouin⁴, K. S. Carslaw¹, M. P. Chipperfield¹, R. Hommel^{5,*}, N. L. Abraham^{3,5}, P. Telford^{3,5}, P. Braesicke^{3,5,**}, M. Dalvi^{3,6}, C. E. Johnson⁶, F. O'Connor⁶, O. Morgenstern⁷, J. A. Pyle^{3,5}, T. Deshler⁸, J. M. Zawodny⁹, and L. W. Thomason⁹

¹School of Earth and Environment, University of Leeds LS2 9JT, UK

²CSIRO Marine and Atmospheric Research, Aspendale, Victoria 3195, Australia

³National Centre for Atmospheric Science (NCAS-Climate), UK

⁴Department of Meteorology, University of Reading, Reading, UK

⁵Department of Chemistry, University of Cambridge, Cambridge, UK

⁶Met Office, Exeter, UK

⁷National Institute of Water and Atmospheric Research (NIWA), Lauder, New Zealand

⁸University of Wyoming, Wyoming, USA

⁹NASA Langley Research Center, Hampton, Virginia, USA

* now at: IUP, University of Bremen, Bremen, Germany

** now at: IMK-ASF Karlsruhe Institute of Technology, Karlsruhe, Germany

ACPD

14, 2799–2855, 2014

Simulation of
Pinatubo aerosol in
a CCM

S. S. Dhomse et al.

Title Page

Abstract

Introduction

Conclusions

References

Tables

Figures

◀

▶

◀

▶

Back

Close

Full Screen / Esc

Printer-friendly Version

Interactive Discussion



Received: 15 December 2013 – Accepted: 15 January 2014 – Published: 28 January 2014

Correspondence to: S. S. Dhomse (s.s.dhomse@leeds.ac.uk)

Published by Copernicus Publications on behalf of the European Geosciences Union.



Abstract

We have enhanced the capability of a microphysical aerosol-chemistry module to simulate the atmospheric aerosol and precursor gases for both tropospheric and stratospheric conditions. Using the Mount Pinatubo eruption (June 1991) as a test case, we evaluate simulated aerosol properties in a composition-climate model against a range of satellite and in-situ observations. Simulations are performed assuming an injection of 20 Tg SO₂ at 19–27 km in tropical latitudes, without any radiative feedback from the simulated aerosol. In both quiescent and volcanically perturbed conditions, simulated aerosol properties in the lower stratosphere show reasonable agreement with the observations. The model captures the observed timing of the maximum aerosol optical depth (AOD) and its decay timescale in both tropics and Northern Hemisphere (NH) mid-latitudes. There is also good qualitative agreement with the observations in terms of spatial and temporal variation of the aerosol effective radius (R_{eff}), which peaks 6–8 months after the eruption. However, the model shows significant biases against some observational data sets. Simulated AOD and Surface Area Density (SAD) in the tropics are substantially higher than the gap-filled satellite data products during the first 6 months after the eruption. The model shows consistently weaker enhancement in R_{eff} compared to satellite and in-situ measurements.

Simulated aerosol particle size distribution is also compared to NH mid-latitude in-situ balloon sounding measurements of size-resolved number concentrations. Before the eruption, the model captures the observed profiles of lower stratospheric particle number concentrations with radii larger than 5, 150 and 250 nm (N_5 , N_{150} and N_{250}) very well. However, in the first 6 months after the eruption, the model shows high bias in N_5 concentrations in the lower stratosphere, suggesting too strong nucleation. Following particle growth via condensation and coagulation, this bias in the finest particles propagates into a factor 2 high bias in N_{150} . Our comparison suggests that new particle formation in the initial phase of large eruptions, and subsequent particle growth to

Simulation of Pinatubo aerosol in a CCM

S. S. Dhomse et al.

[Title Page](#)

[Abstract](#)

[Introduction](#)

[Conclusions](#)

[References](#)

[Tables](#)

[Figures](#)

◀

▶

◀

▶

[Back](#)

[Close](#)

[Full Screen / Esc](#)

[Printer-friendly Version](#)

[Interactive Discussion](#)



optically-active sizes, might be playing an important role in determining the magnitude of the climate impacts from volcanoes like Pinatubo.

1 Introduction

Volcanic eruptions can have significant impact on atmospheric composition and climate (e.g. McCormick et al., 1995; Robock, 2000). Powerful explosive eruptions can inject large amounts of SO₂, ash, water vapour and various other chemical species directly into the stratosphere. Volcanic SO₂ injected into the stratosphere is chemically converted to sulphuric acid vapour over a timescale of days to months, causing substantial new particle formation and aerosol growth by condensation. Such a volcanic enhancement of the stratospheric aerosol substantially increases particle concentrations at optically-active sizes (Deshler et al., 2003) which can persist for several years in the case of tropical eruptions. The optically thicker stratospheric aerosol alters the Earth's radiative balance with increased albedo via enhanced back-scattering of solar radiation, cooling the surface and increased absorption of terrestrial long-wave radiation, warming the stratosphere (Labitzke and McCormick, 1992). The efficiency of these direct radiative effects from the enhanced stratospheric aerosol is strongly influenced by its particle size distribution (Lacis et al., 1992; Hansen et al., 1992).

The long-wave radiative heating induced by the thickened aerosol layer modifies the stratospheric circulation (e.g. Young et al., 1994), leading to indirect radiative effects via dynamical changes in ozone and meridional transport, with important implications for surface climate (Robock and Mao, 1992; Graf et al., 1993). Volcanically increased aerosol surface area density (SAD) can also accelerate heterogeneous chemistry perturbing stratospheric NO_y species, halogens and ozone (e.g. Solomon et al., 1996). Quantifying the net impact from these direct and indirect radiative effects is very important to better understand volcanic influences within the historical climate records.

There is an increasing recognition that having a good representation of stratospheric processes is important for climate projections (e.g. Scaife et al., 2012). However,

[Title Page](#)[Abstract](#)[Introduction](#)[Conclusions](#)[References](#)[Tables](#)[Figures](#)[|◀](#)[▶|](#)[Back](#)[Close](#)[Full Screen / Esc](#)[Printer-friendly Version](#)[Interactive Discussion](#)

Simulation of Pinatubo aerosol in a CCM

S. S. Dhomse et al.

[Title Page](#)[Abstract](#)[Introduction](#)[Conclusions](#)[References](#)[Tables](#)[Figures](#)[|◀](#)[▶|](#)[◀](#)[▶|](#)[Back](#)[Close](#)[Full Screen / Esc](#)[Printer-friendly Version](#)[Interactive Discussion](#)

whereas most coupled atmosphere-ocean climate models (e.g. Jones et al., 2011) that carried out historical integrations for CMIP5 (Taylor et al., 2012) included prognostic treatment of tropospheric aerosol, stratospheric aerosol has always been handled separately. Most of these models used prescribed heating rates from Stenchikov et al. (1998) that are based on time-varying aerosol optical depth from Sato et al. (1993). However, most of these models with prescribed aerosol (and heating rates) are not able to capture the dynamical response that have been associated with volcanic eruptions (Driscoll et al., 2012). An increasing number of chemistry-climate models (CCMs) are designed to simulate the evolution of stratospheric ozone (e.g. SPARC, 2010), but there are still few that include a prognostic treatment of the stratospheric aerosol layer. Many CCMs include prescribed aerosol surface area density. Some also use pre-calculated heating rates to account for stratospheric aerosol induced changes during period of volcanically enhanced aerosol loading. Nevertheless CCMs either overestimate or underestimate the El-Chichon (1982) and Mount Pinatubo (1991) eruption related ozone changes compared with the observations (SPARC, 2010, Fig. 8.20). So, there is great need to have consistent representation of stratospheric aerosols in CCMs.

In this paper, we use the composition-climate model UMUKCA (Unified Model – UK Chemistry and Aerosol) to simulate stratospheric aerosol in both quiescent and volcanically perturbed conditions. The model includes the GLOMAP-mode aerosol micro-physics module, enabling the 3-D evolution of the particle size distribution to be quantified. We use the Mount Pinatubo eruption as a test case to evaluate simulated aerosol properties against a range of observational data from the period. Mount Pinatubo erupted in the Philippines (15.1° N, 120.4° E) on 15 June 1991 and was the largest tropical eruption since Krakatoa in 1883. Using daily SO_2 measurements from the TOMS satellite instrument, Bluth et al. (1992) estimated that the eruption injected about 20 Tg of SO_2 into the stratosphere that was chemically converted to sulphuric acid vapour on a timescale of around 35 days. Assuming a 50 % conversion of SO_2 to sulphuric acid by July and using an assumed size distribution and composition to convert the Stratospheric Aerosol and Gas Experiment II (SAGE-II) satellite measurements of aerosol

extinction, McCormick and Veiga (1992) estimated that the total global aerosol loading was increased between 20 to 30 Tg. Baran and Foot (1994) used infrared satellite measurements from the High resolution Infrared Radiation Sounder (HIRS) instrument to derive a timeseries of the global stratospheric aerosol mass loading, finding a peak of 5 21 Tg in September 1991 with values in excess of 15 Tg persisting until November 1992 and much earlier and steeper decay in the tropics than Northern Hemispheric mid-latitudes. Monthly balloon soundings of total and size-resolved particle concentrations carried out at Laramie, Wyoming (e.g. Deshler, 1994) showed that although substantially enhanced particle concentrations were detected in the lower-most stratosphere 10 by mid-July, the main part of the volcanic plume was only transported to Northern Hemisphere (NH) mid-latitudes several months later.

There have been many previous global modelling studies to simulate the evolution of stratospheric aerosol following the Pinatubo eruption. However most have use aerosol schemes that simulate only the evolution of aerosol mass, prescribing a fixed particle size distribution for sedimentation and radiative effects (e.g. Timmreck et al., 1999; 15 Oman et al., 2006; Aquila et al., 2012; Arfeuille et al., 2013). However, size-resolved stratospheric aerosol modules which include microphysical processes such as new particle formation, coagulation and condensation have also been developed. The first Pinatubo aerosol microphysics simulations were carried out in two-dimensional models (Bekki et al., 1994, 1996; Weisenstein et al., 1997) with single-moment sectional 20 schemes where mass in numerous size bins is transported. More recently several 3-D general circulation models with aerosol microphysics schemes have also been used, to predict sedimentation and changes in radiative forcing in conjunction with the evolving stratospheric particle size distribution (e.g. Timmreck, 2001; Toohey et al., 2011; 25 English et al., 2012, 2013).

Despite the diversity in model complexities, most of these studies evaluated their simulations against a limited set of observational data sets, primarily AODs derived using Advanced Very High Resolution Radiometer (AVHRR) and Stratospheric Aerosol and Gas Experiment (SAGE II) measurements. Using a mass-based prognostic strato-

Title Page	
Abstract	Introduction
Conclusions	References
Tables	Figures
◀	▶
◀	▶
Back	Close
Full Screen / Esc	
Printer-friendly Version	
Interactive Discussion	



Simulation of Pinatubo aerosol in a CCM

S. S. Dhomse et al.

[Title Page](#)

[Abstract](#)

[Introduction](#)

[Conclusions](#)

[References](#)

[Tables](#)

[Figures](#)

◀

▶

◀

▶

[Back](#)

[Close](#)

[Full Screen / Esc](#)

[Printer-friendly Version](#)

[Interactive Discussion](#)



spheric aerosol module in a middle-atmosphere version of the ECHAM4 climate model, Timmreck et al. (1999) showed that the two distinct maxima in AOD apparent in AVHRR and SAGE II based AOD could be simulated, but the model failed to simulate slow AOD decay a few months after the eruption. Similarly, using an offline 3-D chemical transport model, Pitari and Mancini (1999) could simulate SH AOD reasonably well but their model simulations were biased low in the tropical and NH AOD, a few months after the eruption. Aquila et al. (2012), used a mass-based aerosol scheme in a global aerosol transport model, but the model-simulated AOD was slightly lower than AVHRR immediately after the eruption, with better agreement for the later period. Using a sectional aerosol microphysics module, English et al. (2013) achieved good agreement with NH mid-latitude AOD against AVHRR immediately after the eruption but their modelled AOD decayed too rapidly in later months. They compared the aerosol effective radius (R_{eff}) evolution against observations from SAGE II and in-situ measurements (for e.g. Russell et al., 1996; Bauman et al., 2003), finding peak values in the model NH tropical stratosphere occurred earlier than in the observations. Some of these model-observation biases in earlier studies may be linked with the transport related issues (e.g. the lack of a Quasi-Biennial Oscillation, QBO) in the underlying GCM, whereas some may be linked to the simplified treatment of the particle size distribution. Other causes such as interactions with ash, or missing minor eruptions such as Mount Hudson in Chile (September 1991) have also been suggested.

Although they have near-global spatial extent, satellite measurements of AOD and R_{eff} constrain only integrated stratospheric aerosol properties over the full particle size range. Balloon-borne measurements (e.g. Deshler, 1994) enable a closer examination of the particle size distribution, but are available at only a small number of sites.

Here, we use both satellite and balloon-borne measurements to evaluate the UMUKCA simulated stratospheric aerosol properties, and seek to better understand the source of model biases. In Sect. 2 we describe the model, including the experimental set-up and the developments to the aerosol and chemistry schemes which extend its applicability to both stratospheric and tropospheric conditions. Section 3 describes

the measurements that are used to evaluate the model. Results and discussion about potential causes of model-observation biases are presented in Sect. 4 and 5, respectively. Summary and major conclusions are presented in Sect. 6.

2 Model description

- 5 We use an updated version of the stratospheric version of the UMUKCA composition-
climate model originally described in Morgenstern et al. (2009) and evaluated in
SPARC (2010). It is a high-top low resolution version of the Hadley Centre Global En-
vironmental Model (Hewitt et al., 2011) as used by Braesicke et al. (2013) and Telford
et al. (2013). Although UKCA is designed to apply the radiative effects of the simulated
10 aerosol, O₃, CH₄, N₂O and other gases to feedback on the model, in present simula-
tions only the simulated O₃ is radiatively coupled. We run UMUKCA in an atmosphere-
only configuration whereby sea-surface temperature and sea-ice fields are prescribed
from the AMIP time-varying dataset (Hurrell et al., 2008). The simulations are carried
out at N48L60 resolution, which is 2.5° × 3.75° in latitude and longitude with 60 vertical
15 hybrid-height levels from the surface to 84 km. Telford et al. (2009) used a previous
version of the model to study effects of the Pinatubo eruption on the stratospheric
ozone and found that modelled total ozone changes with specified dynamics showed
reasonable agreement with the observations.

To simulate stratospheric aerosol precursor gas phase species, we have extended the existing UKCA stratospheric chemistry scheme to include sulphur chemistry (see Sect. 2.1). The coupling to the GLOMAP-mode aerosol microphysics module (Mann et al., 2010), and its adaptation for stratospheric conditions, is described in Sect. 2.2. Surface emissions of NO_x, CO and HCHO are from the RCP 4.5 scenario. The lower boundary conditions used to determine surface mixing ratios of CH₄, N₂O, CFC-11 (CFCl₃) and CFC-12 (CF₂Cl₂) are from WMO (2011). Minor CFCs (other than CFC-11 and CFC-12), that together account for more than 50 % of atmospheric chlorine, are treated implicitly by a lumping approach. CH₃Br is prescribed at the surface, and



Simulation of
Pinatubo aerosol in
a CCM

S. S. Dhomse et al.

[Title Page](#)

[Abstract](#)

[Introduction](#)

[Conclusions](#)

[References](#)

[Tables](#)

[Figures](#)

[◀](#)

[▶](#)

[◀](#)

[▶](#)

[Back](#)

[Close](#)

[Full Screen / Esc](#)

[Printer-friendly Version](#)

[Interactive Discussion](#)



its abundance is increased to account for halons and very short-lived species (VSLs) which are not treated in the chemistry scheme. This increases CH_3Br concentrations by about a factor of 2 (Morgenstern et al., 2010). Heterogeneous chemical reactions are driven by a prescribed climatology of aerosol surface area density produced for the SPARC Assessment of the Stratospheric Aerosols Report (SPARC, 2006). The calculated aerosols do not influence the model heating rates or ozone chemistry. For the added sulphur species, surface and higher altitude 2-D emissions sources of anthropogenic SO_2 are included following the IPCC AR5 inventory for the year 2000 (Lamarque et al., 2010). A 3-D source from passively degassing volcanoes from Andres and Kasgnoc (1998) is also included. Marine surface emissions of DMS are determined by wind speed using a seawater concentration climatology of Kettle and Andreae (2000) with the sea-air exchange function of Liss and Merlivat (1986). For OCS, which has tropospheric lifetime of about two years (Montzka et al., 2007), we do not include an emissions source, but instead apply a fixed surface boundary condition of 550 pptm.

2.1 Stratospheric chemistry extended for a sulphur cycle

The existing UMUKCA stratospheric chemistry scheme (Morgenstern et al., 2009) covers the oxidation of CH_4 and CO , with chlorine and bromine chemistry and their interaction with HO_x , NO_x and O_x cycles including heterogeneous reactions on polar stratospheric clouds (PSCs) and liquid sulfate aerosols which is based on Chipperfield and Pyle (1998). Here, we have extended the scheme to also include a stratospheric aerosol precursor chemistry scheme based on that used by Weisenstein et al. (1997) with updates to reaction rates from Sander et al. (2006). The added chemistry includes the steady background source of SO_2 from OCS, which principally maintains the stratospheric aerosol during volcanically quiescent periods (e.g. Carslaw and Kärcher, 2006). Also included are photolysis reactions for H_2SO_4 and SO_3 , which occur above about 30 km and lead to a reservoir of SO_2 building up during polar winter, leading to new particle formation in polar spring (Mills et al., 2005). The chemistry is integrated with the ASAD chemical integration package (Carver et al., 1997) with the Newton

Raphson sparse-matrix solver from Wild et al. (2000). Photolysis rates are calculated using the FAST-JX online photolysis (Neu et al., 2007) following the implementation described in Telford et al. (2013). The cross section of H_2SO_4 is assumed analogous to the cross section of HCl, at a fraction of 0.016, following the method of Bekki and Pyle (1992). Gas-phase production of H_2SO_4 is passed to the GLOMAP aerosol scheme to update the gas phase H_2SO_4 tracer on the short “competition timestep” used for nucleation and condensation (see Sect. 2.2). Aqueous sulphate production in (tropospheric) liquid clouds is also passed to the GLOMAP module for growth of accumulation and coarse soluble particles.

10 2.2 The aerosol microphysics module adapted for the stratosphere

The GLOMAP aerosol microphysics module was developed as a component of the TOMCAT 3-D offline Chemical Transport Model (Chipperfield, 2006) with both 2-moment sectional (Spracklen et al., 2005) and 2-moment modal versions (Mann et al., 2010) available. The faster modal scheme (GLOMAP-mode) was specifically designed 15 for longer integrations within UMUKCA and applies similar aerosol microphysics representations as the sectional scheme but with the size distribution parameterised into 7 log-normal modes, being similar in framework to that used in ECHAM-HAM (e.g. Stier et al., 2005). The GLOMAP-mode scheme produces aerosol properties in good agreement with the more sophisticated sectional scheme under most conditions (Mann et al., 2012).

The seven modes used by GLOMAP-mode are a nucleation mode, and Aitken, accumulation and coarse mode aerosol in both soluble and insoluble species. The insoluble modes receive emissions of particles composed of a mixture of black carbon and organic carbon (Aitken-insoluble) or composed entirely of dust (accumulation and coarse insoluble). Since we are focussed on the evolution of the stratospheric aerosol layer 25 after Pinatubo, for this work we use only the four soluble modes and treat only sulphate and sea salt components, the latter included to give reasonable representation of tropospheric aerosol optical properties. Thus far, the GLOMAP aerosol scheme has been

[Title Page](#)

[Abstract](#)

[Introduction](#)

[Conclusions](#)

[References](#)

[Tables](#)

[Figures](#)

◀

▶

[Back](#)

[Close](#)

[Full Screen / Esc](#)

[Printer-friendly Version](#)

[Interactive Discussion](#)



[Title Page](#)

[Abstract](#)

[Introduction](#)

[Conclusions](#)

[References](#)

[Tables](#)

[Figures](#)

[◀](#)

[▶](#)

[◀](#)

[▶](#)

[Back](#)

[Close](#)

[Full Screen / Esc](#)

[Printer-friendly Version](#)

[Interactive Discussion](#)



used to simulate tropospheric aerosol. For this work, the scheme has been updated to apply different methods for the calculation of water uptake, particle density, vapour condensation and new particle formation, for all model levels above the upper troposphere (pressures below 150 hPa).

5 2.2.1 Water uptake

In the standard version of GLOMAP-mode described by Mann et al. (2010), the water uptake to the soluble modes is calculated using the ZSR approach (Zdanovskii, 1948; Stokes and Robinson, 1966) using water activities based on binary electrolyte solutions. In the stratosphere however, aqueous sulphuric acid solution droplets form even 10 at very low relative humidity. We therefore apply the analytical expression of Carslaw et al. (1995) at pressures lower than 150 hPa to calculate water content based on the H_2SO_4 mole fraction for the binary aqueous sulphuric acid solution droplets. At 225 K and 101 hPa, the composition of the solution is 74.5 % H_2SO_4 and 25.5 % water, approximating the 75 % weight fraction assumed in some studies (e.g. Stenchikov et al., 15 1998; Oman et al., 2006).

2.2.2 Particle density

As composition of the aqueous sulphuric acid solution droplets also affects their density, we modified GLOMAP-mode for the stratosphere. For pressures lower than 150 hPa, density values for each mode are replaced with the values from a look-up 20 table based on the measurements of Martin et al. (2000) as a function of the sulphuric acid weight-fraction.

2.2.3 Condensation and vapour pressure of H_2SO_4

In all previous versions of the GLOMAP aerosol module, gas phase H_2SO_4 partitions into the particle phase assuming zero vapour pressure, i.e. the transfer is represented 25 as a condensation process. Although this approach is entirely appropriate in tropo-

[Title Page](#)[Abstract](#)[Introduction](#)[Conclusions](#)[References](#)[Tables](#)[Figures](#)[|](#)[|](#)[◀](#)[▶](#)[Back](#)[Close](#)[Full Screen / Esc](#)[Printer-friendly Version](#)[Interactive Discussion](#)

spheric conditions, above $\sim 25\text{--}30\text{ km}$, the vapour pressure of H_2SO_4 can become significant as the temperatures are high enough that sulphuric acid droplets rapidly evaporate (Hamill et al., 1997; Hommel et al., 2011).

The H_2SO_4 , vapour pressure over a flat surface p is given by Eq. (1) (Ayers et al., 5 1980).

$$\ln(-p) = -(10156/T) + 16.259 + (\mu - \mu^0)/RT \quad (1)$$

Where p is in atmospheres, R is the universal gas constant, μ is chemical potential of H_2SO_4 in a solution at the given composition and μ^0 that of pure acid, and $\mu - \mu^0$ is fitted 10 from experimental data by Giauque et al. (1960). Eq. (1) calculated at 360 K ($p_{360\text{K}}$) is then used to give the vapour pressure for the much lower stratospheric temperatures following Kulmala and Laaksonen (1990):

$$\ln(p_{\text{H}_2\text{SO}_4}) = \ln(p_{360\text{K}}) + \frac{\Delta H_v(360\text{K})}{R} \left[-\frac{1}{T} + \frac{1}{360} + \frac{0.38}{905 - 360} \cdot \left(1 + \ln \frac{360}{T} - \frac{905}{T} \right) \right] \quad (2)$$

15 The reference point 360 K is the base temperature at which Ayers et al. (1980) measured the saturation vapour pressure, 905 K is the critical temperature, and $\Delta H_v(360\text{K})/R$ is set to 10 156 as in Kulmala and Laaksonen (1990).

In this study we do not allow particle evaporation, but modify the existing GLOMAP approach (e.g. Mann et al., 2010) so that condensation of H_2SO_4 proceeds according 20 to the vapour pressure deficit (neglecting the Kelvin effect). This ensures that gas phase H_2SO_4 produced in the upper stratosphere only condenses to the aerosol when the vapour is supersaturated.

2.2.4 New particle formation

Previous versions of GLOMAP (e.g. Mann et al., 2010) allowed formation of new 25 $\text{H}_2\text{SO}_4\text{-H}_2\text{O}$ particles based on the Kulmala et al. (1998) parameterization for binary homogeneous nucleation. This is only applicable at temperatures in the range

233–298 K. Vehkamäki et al. (2002) suggested that conditions for nucleation are also favourable at ~ 200 K in the upper tropical troposphere and they updated the Kulmala et al. (1998) parameterization to be applicable down to lower temperatures and humidities. To allow GLOMAP-mode to be applied in both tropospheric and stratospheric conditions, we have incorporated the Vehkamäki et al. (2002) parameterisation, and used it within the recommended ranges of temperature (190 to 305 K) and H_2SO_4 concentration (10^4 to 10^{11} cm^{-3}). Note that we also use the expression of Kerminen and Kulmala (2002) to convert the “real” nucleation rate from Vehkamäki et al. (2002) into an “apparent nucleation rate” at 3 nm.

2.2.5 Size Distribution

Balloon-borne optical particle counter and condensation nucleus counter measurements in the mid-latitude stratosphere in the 1990s (e.g. Deshler et al., 2003) suggest a bimodal size distribution with the first mode at about 50–150 nm radius with σ_g between 1.6 and 1.8 and a larger much narrower mode ($\sigma_g \sim 1.2$) at around 300–800 nm radius that is weak in volcanically quiescent conditions but much stronger (in number) following the Pinatubo eruption (e.g. Carslaw and Kärcher, 2006). After such large volcanic eruptions, a significant proportion of stratospheric sulphuric acid aerosol droplets grow to super-micron sizes. For example Deshler et al. (2003) show that in March 1993 (21 months after the Pinatubo eruption), in the NH mid-latitude lower stratosphere there was a 6 km layer (12–18 km) with the number concentration of particles with radii larger than 500 nm greater than 1 cm^{-3} . Such coarse particles have grown from their original size of around 1 nm due to coagulation and gas-to-particle transfer of sulphuric acid. Modal microphysics schemes such as GLOMAP-mode represent this condensational and coagulational growth, but must use a technique referred to as “mode-merging” (e.g. Binkowski and Roselle, 2003) to transfer particles to adjacent larger modes following strong growth. In this case of a large volcanic eruption, the mode-merging must transfer particles first from the nucleation mode to the soluble Aitken mode, and following further growth up to the soluble accumulation mode and then to the soluble coarse



Simulation of Pinatubo aerosol in a CCM

S. S. Dhomse et al.

[Title Page](#)

[Abstract](#)

[Introduction](#)

[Conclusions](#)

[References](#)

[Tables](#)

[Figures](#)

◀

▶

[Back](#)

[Close](#)

[Full Screen / Esc](#)

[Printer-friendly Version](#)

[Interactive Discussion](#)



mode. In each case, when particles are received from the adjacent smaller mode, the transferred number and mass is added to that existing in the mode, with the mean size re-formulated according to the prescribed standard deviation of the mode (σ_g).

- Kokkola et al. (2009) compared size distributions simulated by a modal and three sectional schemes in a box model. While the four models agreed well in background stratospheric conditions, in volcanically perturbed conditions, the size distributions were found to be better represented with narrower mode widths. In particular, with the original coarse mode σ_g of 2.0, they found the modal scheme over-predicted the R_{eff} compared to a reference sectional scheme with a large number of bins. Niemeier et al. (2009) used an improved version of the same modal microphysics scheme whereby σ_g for the accumulation soluble mode was reduced to 1.2 and the coarse mode was de-activated.

Here we are applying the modal GLOMAP scheme to volcanically-perturbed stratospheric conditions, and also using the same modes to also represent tropospheric aerosol. In the troposphere, the coarse soluble mode in GLOMAP-mode is almost exclusively containing sea-salt, and the scheme has followed Wilson et al. (2001) and Vignati et al. (2004) in using a value of 2.0 for σ_g in this mode, which are based on values given in D'Almeida et al. (1991). However, Heintzenberg et al. (2004) present size distribution observations over several fields campaigns in the marine boundary layer which find a median value of coarse mode σ_g at 1.4.

To best represent coarse particles in both tropospheric and stratospheric conditions, we reduce σ_g for the coarse soluble mode to be 1.4 rather than 2.0. We retain the σ_g value of 1.4 for the soluble accumulation mode in GLOMAP-mode, as reduced by Mann et al. (2012) from the value of 1.59 used in Mann et al. (2010) to better compare with size distributions simulated by the sectional scheme and with observations. We retain the $\sigma_g = 1.59$ values for the nucleation and Aitken modes. The narrowed coarse soluble mode σ_g of 1.4 matches that for the accumulation soluble mode, which is desirable numerically when the mode-merging algorithm transfers particles between the two modes in strong particle growth conditions.

2.3 Experimental setup

To examine the perturbation to the stratospheric aerosol layer that occurred after the Pinatubo eruption, we performed two simulations with (run Pinatubo) and without (run no-Pinatubo) related SO₂ injection. For run Pinatubo, the model is configured to inject 5 20 Tg of SO₂ into the tropical stratosphere on 15th June 1991 between 19 and 27 km. Satellite observations of SO₂ after the eruption (Bluth et al., 1992) show that the plume initially dispersed southwards crossing the equator within two weeks. As described in Sect. 2, the simulated aerosol is not radiatively coupled to the atmospheric dynamics, which is believed to be an important limitation in simulating the initial dispersion of 10 the Pinatubo plume correctly (Young et al., 1994). Consequently, to ensure we closely match the initial spatial distribution of the aerosol cloud, as in Timmreck et al. (1999) we apply the SO₂ injection spread across eight model grid boxes between 0–20° N 120.5° E. The aerosol and gas phase sulphur species had 8 yr spin-up from an initialisation with zero aerosol and gas phase species, with other gases from the UMUKCA 15 REF-C1 integration from the SPARC Lifetimes Assessment Report (SPARC, 2013), representative of 1990 conditions.

A key mode of inter-annual variability in the tropical lower stratosphere is the observed QBO of zonal winds between easterly and westerly phases, which occurs with a period of 22 to 34 months with an average of 28 months (Andrews et al., 1987; 20 Baldwin et al., 2001). Using satellite observations, Trepte and Hitchman (1992) showed the important role the QBO phase played in determining the initial dispersion of the Pinatubo plume.

For this experiment, we picked the initialisation year such that lower stratospheric winds in the model were in the easterly phase of the QBO, as at the time of the actual eruption. Figure 1a shows the time evolution of the model monthly and zonal-mean zonal wind in the tropics (15°S–15°N) against those from the ERA interim reanalysis from 1990 until 1995 (Fig. 1b Dee et al., 2011). At the time of the eruption (15 June 1991), the model has an easterly QBO phase with easterly winds stronger 25

[Title Page](#)[Abstract](#)[Introduction](#)[Conclusions](#)[References](#)[Tables](#)[Figures](#)[◀](#)[▶](#)[Back](#)[Close](#)[Full Screen / Esc](#)[Printer-friendly Version](#)[Interactive Discussion](#)

Simulation of Pinatubo aerosol in a CCM

S. S. Dhomse et al.

[Title Page](#)

[Abstract](#)

[Introduction](#)

[Conclusions](#)

[References](#)

[Tables](#)

[Figures](#)

[|◀](#)

[▶|](#)

[◀](#)

[▶|](#)

[Back](#)

[Close](#)

[Full Screen / Esc](#)

[Printer-friendly Version](#)

[Interactive Discussion](#)



than 10 ms^{-1} above 33 hPa, agreeing well with the ERA-interim tropical zonal wind profile at that time. This model easterly QBO phase continues until around April 1992 (at 30 hPa), the shift to westerly flow occurring slightly earlier than in ERA-interim, which continues until around September 1992. The semi-annual oscillation in the tropical middle and upper stratosphere is also well represented in the model.

How rapidly the Pinatubo-enhanced stratospheric aerosol layer returns to pre-eruption levels is strongly influenced by the strength of the model stratospheric circulation. Sedimentation of particles is also important as it moves particles closer to the tropopause where they can be removed by stratospheric-tropospheric exchange (e.g. Deshler, 2008). A common metric used to assess stratospheric transport in chemistry-climate models (e.g. Strahan et al., 2011) is the mean stratospheric age of air.

Figure 1c shows the latitude and altitude distribution of the model zonal-mean age of air (for 1991–2000) and Fig. 1d compares the model age of air at 50 hPa against that derived from aircraft observations of the long-lived tropospheric source gases SF₆ and CO₂ (Hall et al., 1999). The values from other composition-climate models participating in the recent CCMVal lifetime assessment (Chipperfield et al., 2013) are also shown for reference. In the tropics, the model age of air agrees well with the observations, but at mid- and high latitudes there is a low bias compared to the observations; up to 1 yr too young air at high latitudes. The low bias in mid-latitude age-of-air indicates that model may have too rapid meridional poleward transport as well as stronger STE. In turn, such a mixing can cause too fast removal of aerosol from the stratosphere into the mid-high latitude troposphere, and should be considered when drawing inference from the evaluation of the model post-Pinatubo stratospheric aerosol decay.

3 Measurements

To evaluate the UKCA simulations, we use measurements from the SAGE II instrument (McCormick and Veiga, 1992), which was launched on the Earth Radiation Budget Satellite (ERBS) in 1984. SAGE II was a seven-channel Sun photometer oper-

ated in solar occultation mode with a vertical resolution of about 0.5 km. Spectral windows were centred at 385, 448, 453, 525, 600, 940 and 1020 nm. For evaluating the model stratospheric aerosol optical depth, we use the gap-filled SAGE-II (V6.2) product (Hamill et al., 2006) produced for ASAP (Assessment of Stratospheric Aerosol Properties SPARC, 2006). Simulated aerosol extinction is compared against the recently updated version (V7.0) of the SAGE-II data (Damadeo et al., 2013). We also compare to the SAGE-derived SAD product (Thomason et al., 1997) that is obtained from <http://www.sparc-climate.org/data-center/data-access/asap/>. Simulated SAD is also compared against the recently available SAD data Arfeuille et al. (2013) which was created using SAGE II V7.0 data, and is provided for the Chemistry Climate Model Initiative (CCMI) simulations. Further evaluation of the post-Pinatubo simulated aerosol optical depth (AOD) evolution was carried out by comparing to that measured by the Advanced Very High Resolution Radiometer (AVHRR/2), which was onboard on the National Oceanic and Atmospheric Administration (NOAA/11) satellite. For details see http://www.nsof.class.noaa.gov/release/data_available/avhrr/index.htm. The AVHRR instrument measures the reflectance of the Earth in five spectral bands centred around 0.6, 0.9, 3.5, 11 and 12 μm .

To examine the simulated particle size distribution that underpins the model aerosol optical properties, we also compare to profile measurements of size-resolved number concentration made at Laramie, USA (Deshler et al., 2003). The balloon-borne system includes a Condensation Nucleus Counter (CNC) to measure the concentrations of particles larger than 10 nm and an optical particle counter (OPC Deshler et al., 1992) to measure size-resolved particle concentrations in several size ranges in the accumulation and coarse regions of the size spectrum. The OPC is a light counter to derive integrated size distribution from measured aerosol scattering in the forward direction. The standard OPC design gives integral number concentrations larger than 150 nm and 250 nm radius, and has been used in balloon sounding measurements of the stratospheric aerosol since 1963 (Rosen, 1964), also giving important information about the stratospheric aerosol changes induced by the 1980 Mount St. Helen's

Simulation of Pinatubo aerosol in a CCM

S. S. Dhomse et al.

[Title Page](#)

[Abstract](#)

[Introduction](#)

[Conclusions](#)

[References](#)

[Tables](#)

[Figures](#)

◀

▶

◀

▶

[Back](#)

[Close](#)

[Full Screen / Esc](#)

[Printer-friendly Version](#)

[Interactive Discussion](#)



eruption (Hofmann and Rosen, 1982). Deshler et al. (1992) present the measurements taken in the first few months after the June 1991 Pinatubo eruption, with most balloon flights using this original 2-channel OPC. An enhanced OPC, using an increased scattering angle, measured concentrations in 8 size channels for radii larger than 150 nm to around 10 microns. The 8-channel OPC had been developed shortly before the eruption, and became the default measuring system a few months after the eruption. The measurement capabilities were later further enhanced to measure up to twelve size ranges (see Deshler et al., 2003).

4 Results

- Figure 2 shows the January 1991 to December 1994 time-evolution of the total global column mass burden of sulphur in the gas phase (as SO_2 , red) and in the aerosol particle phase (blue) from our Pinatubo and no-Pinatubo simulations. Separate lines indicating the UTS aerosol sulphur burden (Upper Tropospheric and Stratosphere) and that in the mid- and lower stratosphere are also shown. Without Pinatubo (dotted lines), the global SO_2 and aerosol sulphur burden timeseries are dominated by anthropogenic emissions which are mostly emitted in NH mid-latitudes. Oxidant concentrations are highest during the summer due to stronger photochemistry, which leads to efficient conversion of SO_2 to aerosol sulphate. During the NH summer, only 10 % of the total sulphur burden comes from SO_2 , compared to around 50 % during winter. In our model, 30–40 % of the total aerosol sulphur burden (around 0.5 Tg S) is in the stratosphere, which is considerably higher than the 17% (15 Tg S) found by Hommel et al. (2011). Tropospheric aerosol burdens are also higher than other models Textor et al. (e.g. 2006) at around 1.25 Tg S on the annual mean. For the Pinatubo simulation, the global SO_2 burden peaks at 5.75 Tg for the July 1991 monthly-mean. However, note that the June monthly-mean SO_2 burden of 4.75 Tg included 15 days of simulation before the eruption (which had zero stratospheric SO_2), and can thus be approximated as around 9 Tg of sulphur.

Title Page	
Abstract	Introduction
Conclusions	References
Tables	Figures
◀	▶
◀	▶
Back	Close
Full Screen / Esc	
Printer-friendly Version	
Interactive Discussion	



Simulation of Pinatubo aerosol in a CCM

S. S. Dhomse et al.

[Title Page](#)

[Abstract](#)

[Introduction](#)

[Conclusions](#)

[References](#)

[Tables](#)

[Figures](#)

◀

▶

[Back](#)

[Close](#)

[Full Screen / Esc](#)

[Printer-friendly Version](#)

[Interactive Discussion](#)



The July mean SO_2 burden can be considered as representative of the centre of the month, i.e. about 30 days after the eruption. Subtracting the SO_2 mass from the no-Pinatubo run (which is all in the troposphere), gives 5.4 Tg S, suggesting 4.6 of the emitted 10 Tg S emitted as SO_2 has been chemically converted to sulphuric acid over the 30 days. We therefore estimate the e-folding timescale for conversion of SO_2 into sulphuric acid aerosol as 30 divided by $\ln(10/5.4)$ which is 49 days. Bluth et al. (1992) derived an e-folding timescale of 35 days from the TOMS satellite SO_2 measurements, but present this as a tentative estimate. McCormick and Veiga (1992) derived an approximate aerosol sulphur burden assuming a 50 % conversion from SO_2 to H_2SO_4 by the end of July, which corresponds to an e-folding timescale of 43 days. Oman et al. (2006) found an SO_2 e-folding conversion timescale of 35 days in their model, which used fixed OH concentrations. The Bekki (1995) timescale is 40 days, based on 2-D model simulations with stratospheric sulphur and oxidant chemistry, thus accounting for the depletion of oxidants, as in our study.

The peak in global aerosol sulphur burden occurs 3 months after the eruption in September, in agreement with Baran and Foot (1994). We find a maximum total aerosol burden of 10.2 Tg of sulphur, with 9 Tg of sulphur in the stratosphere, or 36 Tg aerosol mass assuming 75 % sulphuric acid composition, slightly higher than the 21.5 Tg (5.4 Tg of sulphur) estimated by Baran and Foot (1994). The model global aerosol burden reduced to 3.5 Tg of sulphur by June 1992 (12 months after the eruption) suggesting an e-folding time for the model aerosol mass of 15.8 months; slightly longer than the range of 12–14 months estimated by Baran and Foot (1994) and Bluth et al. (1997).

Figure 3 shows vertical profiles of mixing ratios of the three key gas phase sulphur species OCS, SO_2 , H_2SO_4 , and of sulphuric acid in the particle phase ($\text{Aer}_-\text{H}_2\text{SO}_4$) The left and right panels are for mean profiles in the tropics (15°S – 15°N) and mid-latitudes (35 – 60°N), respectively with the top and bottom rows indicating the means for July 1991 and October 1991, selected as they show the initial period when the SO_2 is oxidised to H_2SO_4 vapour, and the period when the peak global aerosol burden oc-

Simulation of Pinatubo aerosol in a CCM

S. S. Dhomse et al.

[Title Page](#)[Abstract](#)[Introduction](#)[Conclusions](#)[References](#)[Tables](#)[Figures](#)[|◀](#)[▶|](#)[Back](#)[Close](#)[Full Screen / Esc](#)[Printer-friendly Version](#)[Interactive Discussion](#)

The October mean SO_2 profile is still strongly enhanced (factor 100) in the tropics with the P- H_2SO_4 enhancement only slightly higher than in July but over a much deeper layer. This tropical enhancement in both SO_2 and Aer- H_2SO_4 propagates up to above 40 km, although the aerosol enhancement is unrealistic as it will in reality have evaporated at those altitudes. It is interesting that the October 1991 tropical gas phase H_2SO_4 profile actually shows lower values than in quiescent conditions in the main part of the plume (15–30 km), due to the condensation sink to aerosol being so much stronger. By contrast above 30 km the increase in vapour pressure shuts off the condensation sink leading to the H_2SO_4 vapour concentrations being higher than quiescent at those altitudes. The October 1991 NH mid-latitude SO_2 and Aer- H_2SO_4 profiles show only moderate enhancement suggesting the easterly phase of the QBO has prevented transport of Pinatubo-enhanced air masses.

Figure 4a shows the time evolution of the model mid-visible stratospheric AOD, with Fig. 4b and c showing the mid-visible AOD measured from AVHRR and SAGE II. Since AVHRR is a nadir viewing instrument, the derived AODs are from the full column aerosol (covering both troposphere and stratosphere). Hence, in Fig. 4b we have subtracted monthly-mean AODs for the year prior to the eruption (as in Aquila et al., 2012). Note that the SAGE-II derived AOD is lower than AVHRR, due to the measured extinction saturating during the very high loading period after Pinatubo (Hamill et al., 2006). Overall, there is good qualitative agreement between the model and satellite AOD distributions. For example, there is high AOD after the eruption centred around the equator with peak AOD in September 1991 in both the model and the two satellite datasets. However, the model feature is narrower, confined between 10° N and 10° S. Another well-captured feature in the model is that there is no significant enhancement of AOD in NH mid-high latitudes until October 1991. The model does not capture the observed AOD enhancements in the Southern Hemisphere (SH). Extinction profile measurements from SAGE-II between July and September show (e.g. McCormick et al., 1995) that transport to the SH occurred above about 24 km. Aquila et al. (2012) highlighted the importance of resolving the enhanced tropical upwelling which occurred due to the

Simulation of Pinatubo aerosol in a CCM

S. S. Dhomse et al.

Title Page

Abstract

Introduction

Conclusions

References

Tables

Figures

Page 1

ANSWER



Back

Close

Full Screen / Esc

[Printer-friendly Version](#)

Interactive Discussion



Simulation of Pinatubo aerosol in a CCM

S. S. Dhomse et al.

[Title Page](#)

[Abstract](#)

[Introduction](#)

[Conclusions](#)

[References](#)

[Tables](#)

[Figures](#)

◀

▶

◀

▶

[Back](#)

[Close](#)

[Full Screen / Esc](#)

[Printer-friendly Version](#)

[Interactive Discussion](#)



long-wave absorption by the relatively larger stratospheric aerosol after the Pinatubo eruption. As explained in Sect. 2, in these simulations we do not radiatively couple the simulated aerosol with the model dynamics, which likely explains this discrepancy. Another reason could be the eruption of Cerro Hudson in Chile (46° S, 73° W), which occurred from 12–15 August 1991, and is not included in our simulations.

Figure 5 shows model and SAGE-II aerosol extinctions at 32, 25 and 20 km in the tropics (20° S– 20° N). We choose these altitudes to allow comparison with the evaluation presented in Weisenstein et al. (2006, Fig. 6.20) for other stratospheric aerosol models. Here we compare extinction in the mid-visible (panels a to c) as well as the near infrared (panels d to f). We use the updated v7.0 SAGE-II dataset and the profiles shown are averages between 20° S and 20° N. Monthly mean observed values are calculated based on both sunrise and sunset profiles.

At 20 and 25 km, the model captures the general evolution of the tropical mid-visible extinction, with the magnitude and timing of peak values, and the decay timescale, agreeing well with SAGE-II. However, before the eruption, modelled extinctions have a moderate low bias of 30–50 % at these levels. Also, at 25 km, the model extinction reduces sharply after its peak, whereas in the satellite measurements, values plateau for 2–3 months before the decay period begins. At 32 km, simulated extinctions are consistently higher than SAGE, although there are large measurement error bars. The bias may indicate that the model upper injection altitude was too high or be related to the lack of aerosol-induced radiative heating as well as lack of aerosol evaporation in our simulations. As noted above, the SAGE-II instrument saturated in the tropics during this high aerosol loading period and we do not have any observed data points to constrain the simulated mid-visible extinction at 20 km.

At near-infrared wavelengths, the model also agrees fairly well with the observations, although differences are larger than at mid-visible wavelengths. For example, at 20 km, the period of increasing extinction is much longer lasting in the observations than in the model. At 25 km, the model agrees better with the observations, but extinctions are slightly lower than measured by SAGE-II. It is also noticeable that the SAGE-II extinc-

Simulation of Pinatubo aerosol in a CCM

S. S. Dhomse et al.

[Title Page](#)[Abstract](#)[Introduction](#)[Conclusions](#)[References](#)[Tables](#)[Figures](#)[|◀](#)[▶|](#)[◀](#)[▶|](#)[Back](#)[Close](#)[Full Screen / Esc](#)[Printer-friendly Version](#)[Interactive Discussion](#)

tion stays approximately constant at close to the known saturation value of 0.01 km^{-1} for several months at both altitudes.

Figure 6 shows a similar analysis to Fig. 5, but for NH mid-latitudes ($35\text{--}60^\circ \text{ N}$), again to compare against models shown in Weisenstein et al. (2006). At 20 km, there is good agreement between modelled and SAGE II extinctions, although the model appears slightly higher in the first 6 months after the eruption. At 25 km however, the model is consistently higher than the observations, in common with the models participating in the SPARC (2006). A noticeable seasonal cycle is seen in the SAGE-II extinction at 25 km, which is not captured by the model. This might be due to the absence of aerosol evaporation in our simulations. At 32 km the model has a similar evolution to that simulated at 20 and 25 km, whereas the observations indicate very little volcanic enhancement occurred at this level.

Figure 7 compares the vertical and latitudinal distribution of zonal mean SAD against two versions of the satellite derived SAD dataset, for four selected months between May 1991 and May 1992. Before the eruption (May 1991), the model captures the observed SAD very well with a hemispherically symmetric distribution in the lower stratosphere in the range 0.5 to $2 \text{ m}^2 \text{ cm}^{-3}$. For September 1991 (three months after the eruption), although the simulated SAD distribution broadly matches the observed shape, it is up to a factor 5 to 6 too high in the tropics. Also, the model Pinatubo-enhanced SAD plume is too strongly confined to the tropical pipe, whereas in the satellite-derived SAD (Fig. 7d) one can see weak meridional transport to NH and SH sub-tropics at about 20–22 km. Young et al. (1994) show that including the aerosol radiative effects on the model dynamics broadens the latitudinal extent of the Pinatubo cloud, in better agreement with the satellite observations, and this is likely the source of the bias seen here. By January 1992, the model high-bias has reduced to a factor 3–4, and the model shows meridional transport to NH mid-latitudes in the lowermost stratosphere, also seen in the observations. However, the satellite derived SAD suggest meridional transport also occurs to the SH, but at slightly higher altitudes. By May 1992, the model SAD high bias is less than a factor of 2 and the general latitudinal and altitudinal distribution

Simulation of Pinatubo aerosol in a CCM

S. S. Dhomse et al.

[Title Page](#)[Abstract](#)[Introduction](#)[Conclusions](#)[References](#)[Tables](#)[Figures](#)[|◀](#)[▶|](#)[◀](#)[▶|](#)[Back](#)[Close](#)[Full Screen / Esc](#)[Printer-friendly Version](#)[Interactive Discussion](#)

$$R_{\text{eff}} = \frac{\sum_{i=1}^m N_i r_{gi}^3 \exp [9/2(\ln \sigma_i)^2]}{\sum_{i=1}^m N_i r_{gi}^2 \exp [2(\ln \sigma_i)^2]} \quad (3)$$

The two gap-filled SAGE/SAM extinction data products thereby provide 3-D time-varying volume concentration and SAD which together give R_{eff} throughout the Pinatubo period. This record therefore has the potential to give unprecedented information on how the particle size distribution in the stratosphere was perturbed by the eruption. However, again, when comparing the model to the satellite R_{eff} , the limitations associated with the derived product need to be considered. In particular, because of the “blind spot” associated with particles smaller than 50–100 nm, (Hamill et al., 2006) state that since the derived SAD may have an inherent low bias (whereas the derived volume density will be less affected) the derived R_{eff} may overestimate the true value.

Figure 8 shows the evolution of the model zonal-mean R_{eff} at 20 and 25 km compared to that derived by Bauman et al. (2003) from the SAGE-II and CLAES satellite measurements. The general spatial and temporal evolution of the model R_{eff} is in good qualitative agreement with the observations, with values at 20 km larger than at 25 km, likely due to sedimentation. At both altitudes the observations show a gradual decay from peak effective values in around October to December at 20 km and February to March 1992 at 25 km. In the model, the timing of the peak R_{eff} is well captured, but at 25 km, the model peaks later than observed, matching the timing at 20 km. Effective radius values are always higher in the tropics than at mid-latitudes, a feature that is consistent between the model and observations. However, the model values are substantially lower than those derived from the satellite, with maximum model R_{eff} of around 0.4 μm , compared to around 0.6 μm from the satellites.

At 20 km (Fig. 8b), despite combining the two sets of satellite products, there is no observational constraint on the tropical R_{eff} between approximately June 1991 and August 1992, but the overall shape suggests the R_{eff} was likely even larger than 0.6 μm .

Simulation of Pinatubo aerosol in a CCM

S. S. Dhomse et al.

[Title Page](#)

[Abstract](#)

[Introduction](#)

[Conclusions](#)

[References](#)

[Tables](#)

[Figures](#)

◀

▶

[Back](#)

[Close](#)

[Full Screen / Esc](#)

[Printer-friendly Version](#)

[Interactive Discussion](#)



Simulation of Pinatubo aerosol in a CCM

S. S. Dhomse et al.

5 during that period. The model low bias in R_{eff} is apparent at about the same extent at all latitudes and altitudes and before the eruption, which suggests it is not associated with sedimentation, since that would be expected to occur mostly during the highest loading period. There appears to be a more persistent bias in simulated particle size distribution, but it is unclear whether the model has too many small particles, or too few large particles.

To give a stronger observational constraint on the simulated size distribution, we compare the model against balloon-borne CNC and OPC measurements made at Laramie, Wyoming, USA (41° N), see Sect. 3. Figures 9 and 10 compare model profiles of size-resolved number concentrations (larger than a given particle diameter) against those measured by the CNC and OPC. In each case we are comparing a monthly-mean size-resolved particle concentration to a single balloon sounding. Note that whereas the number concentration profiles for particles larger than 5 nm, 150 nm and 250 nm are exactly as measured by the OPC, the larger size channels we have interpolated the observations (linearly in $\log N$ vs. $\log R$ space) onto regular $D_p > 550$ nm, 750 nm and 1000 nm size channels from the irregular size thresholds given in the individual sounding data files.

Figure 9 presents the comparison through August to November 1991, in the period after the Pinatubo plume was first detected as Laramie on 16 July (Deshler et al., 1992). In August and September 1991, the model predicts that the eruption enhanced N_5 , N_{150} and N_{250} between 14 and 20 km compared to the no-Pinatubo run, whereas at higher altitudes the profile remains unperturbed. The region with elevated N_5 , N_{150} and N_{250} profiles matches well with the observations, and indicates efficient transport of air from the tropics in the lowermost stratosphere. Intriguingly, the model predicts that the eruption reduced concentrations of particles at sizes larger than 750 nm. One possible explanation could be that there is reduced growth of background nuclei to these coarse sizes when N_{150} and N_{250} are so high. However, observations from balloon soundings in the post-Pinatubo quiescent period (Deshler et al., 2003) show much lower concentrations of these coarse particles than in our model. Whereas the observations show

Title Page	
Abstract	Introduction
Conclusions	References
Tables	Figures
◀	▶
◀	▶
Back	Close
Full Screen / Esc	
Printer-friendly Version	
Interactive Discussion	



Simulation of Pinatubo aerosol in a CCM

S. S. Dhomse et al.

[Title Page](#)[Abstract](#)[Introduction](#)[Conclusions](#)[References](#)[Tables](#)[Figures](#)[|◀](#)[▶|](#)[◀](#)[▶|](#)[Back](#)[Close](#)[Full Screen / Esc](#)[Printer-friendly Version](#)[Interactive Discussion](#)

- In order to evaluate the model size distribution profile in quiescent conditions, we compare to the Laramie balloon measurements in March 1991 (Fig. 10a). We then probe the longer-timescale evolution of the size distribution through the Pinatubo period, in March 1992, 1993 and 1994 (Fig. 10b, c and d). Before the eruption, the observations show that N_5 decreases with increasing altitude between 12 and 23 km, whereas N_{150} and N_{250} show very little decrease with height. This feature is well captured by the model with N_5 and N_{150} in excellent agreement with the observations in this altitude range, although N_{250} has a slight low bias. Between 25 and 30 km, the observed N_5 profile shows a layer of enhanced concentrations, by around a factor of 10. By contrast the model N_5 profile shows a steady decrease with height in this altitude range, at the same rate as found in the lower stratosphere. The altitude of this sudden N_5 increase corresponds approximately to where temperatures become warm enough for sulphuric acid particles to evaporate, which is not included in our simulations. Gas phase sulphuric acid concentrations are known to increase rapidly with height in this region from balloon-borne ion mass spectrometer measurements (e.g. Arnold et al., 1981). These elevated concentrations of gas phase H_2SO_4 have been shown to cause significant nucleation in the middle-stratosphere (Hommel et al., 2011) which may be the cause of this observed feature.

In March 1992 (Fig. 10b), 9 months after the eruption, the observed particle concentration profiles show major enhancements between 17 and 25 km, compared to March 1991 for all size thresholds 150 nm and larger. By contrast, N_5 has increased only slightly, and is only marginally higher than N_{150} and N_{250} for this month, suggesting most particles have grown larger than 250 nm in this height range. In the model, the lower stratosphere N_5 and N_{150} high biases seen for November 1991 (Fig. 9c) have worsened further, by factors of 8 and 2 respectively. However, the model N_{250} , N_{550} , N_{750} and N_{1000} show much better agreement with the observations.

In March 1993 (Fig. 10c), the observations show clear separation between N_5 and N_{150} , although N_{150} and N_{250} are close together. This indicates the formation of a bimodal size distribution consisting of an external mixture of particles which have grown

Title Page	
Abstract	Introduction
Conclusions	References
Tables	Figures
◀	▶
◀	▶
Back	Close
Full Screen / Esc	
Printer-friendly Version	
Interactive Discussion	



to larger sizes following oxidation of volcanic SO_2 and a separate sub-population of particles less influenced by the eruption. The model continues to show greatly enhanced N_5 compared to the no-Pinatubo simulation profile (dashed line) whereas the observed N_5 profile indicates it has returned to the pre-Pinatubo profile from March 1991. It is interesting that the model N_5 profile for the no-Pinatubo simulation matches well with the observations at this time, further suggesting that particles lower than 150 nm have reverted to background concentrations (whereas the model N_5 is still strongly perturbed). Despite this bias in the finest particles, the model N_{250} and N_{1000} profiles are in good agreement with the observations, although N_{550} and N_{750} are biased low in the lower-most stratosphere. By March 1994 (Fig. 10d) there has been a general decay towards background conditions, and the N_5 bias has reduced, whereas N_{150} continues to be too high throughout the lower stratosphere.

5 Discussion

The comparisons against the balloon measurements (Figs. 9 and 10) show that the model captures the general evolution of the particle size distribution in the stratosphere through the Pinatubo period. The observations indicate how the huge injection of SO_2 led after the eruption to the growth of some particles from an initial size of around 1 nm at formation to sizes larger than 1 μm at peak loading (e.g. Figure 10b), with a long-lasting perturbation to concentrations larger than 150 nm with a complex evolution of R_{eff} (Fig. 8). The shift in the size distribution to a larger R_{eff} will have caused significant changes in the radiative properties of the stratospheric aerosol, with significant absorption of outgoing terrestrial radiation and a decrease in the efficiency of back-scattering of incoming solar radiation. These altered radiative effects illustrate the importance of resolving aerosol particle size changes and subsequent radiative feedbacks in stratospheric composition-climate models and we aim to present them in future studies.

Although the model captures the main features of the observed evolution of the particle size distribution reasonably well, we have seen that simulated particle concentra-

Title Page

Abstract

Introduction

Conclusions

References

Tables

Figures

◀

▶

◀

▶

Back

Close

Full Screen / Esc

Printer-friendly Version

Interactive Discussion



tions in the 5–250 nm size range are too high compared to the observations. There are several possible causes for this model size distribution bias. First, nucleation rates at the very low humidity and temperature conditions in the stratosphere are known to be highly uncertain. The Vehkamäki et al. (2002) parameterization used in this paper is the best available for stratospheric conditions, but is essentially an extrapolation from laboratory measurements at much higher temperatures and humidities, based on classical nucleation theory. Second, the nucleation rate expression is a steep non-linear function of the sulphuric acid concentrations, which may vary considerably in the large global model grid-boxes. An approach sometimes used in global models to represent sub-grid-scale nucleation and growth, is to include a small fraction of the SO_2 emitted as a source of “primary sulphate” particles, with a prescribed size distribution. For example, Dentener et al. (2006) recommend including 2.5 % of SO_2 emitted from passively degassing and explosive volcanoes as primary sulphate with an R_{eff} of around 60 nm. Including such a sub-grid source of particles would also reduce gas phase H_2SO_4 concentrations, since immediately after the eruption there would already be substantial particle surface area density. Lower H_2SO_4 concentrations would hence lead to lower nucleation rates and would also weaken particle growth, which would tend to reduce both N_5 and N_{150} .

To document the nucleation rate occurring in the no-Pinatubo and Pinatubo simulations, we show in Fig. 11 its global distribution, on the zonal-mean, against latitude and altitude over the period July to October 1991. In volcanically quiescent conditions, the model has nucleation occurring mainly in the tropical upper troposphere with negligible new particle formation in the stratosphere. The observed and simulated lower stratospheric N_5 and N_{150} profiles at Laramie in March 1991 (Fig. 10a) are in good agreement, and Fig. 11 indicates that these stratospheric particles were actually formed in the tropical upper troposphere, consistent with the stratospheric aerosol lifecycle described by Hamill et al. (1997). The observations at Laramie indicate that only a small proportion of these nucleated particles grow to sizes larger than 150 nm, with most being at smaller sizes.

Title Page	
Abstract	Introduction
Conclusions	References
Tables	Figures
◀	▶
◀	▶
Back	Close
Full Screen / Esc	
Printer-friendly Version	
Interactive Discussion	



Simulation of Pinatubo aerosol in a CCM

S. S. Dhomse et al.

[Title Page](#)

[Abstract](#)

[Introduction](#)

[Conclusions](#)

[References](#)

[Tables](#)

[Figures](#)

◀

▶

◀

▶

[Back](#)

[Close](#)

[Full Screen / Esc](#)

[Printer-friendly Version](#)

[Interactive Discussion](#)



from Aitken sized particles. We note that in Fig. 7 the model shows highest biases in simulated SAD against the observations during the first few months after the eruption.

6 Summary and conclusions

We have extended the UKCA module to incorporate stratospheric sulphur chemistry and stratospheric microphysical processes. Using stratospheric aerosol changes after the Mt. Pinatubo as a test case, we have evaluated simulated aerosol properties against a wide range of observations in both quiescent and volcanically perturbed conditions. The improvements to the model enable a prognostic treatment of stratospheric aerosol with dynamically varying particle size distribution alongside stratospheric transport and chemistry up to a model top of 84 km.

In general, the model captures the observed distribution and evolution of stratospheric aerosol properties well, in both quiescent and volcanically perturbed conditions. For the Pinatubo test case, the peak in global aerosol mass and decay timescale are captured well, with an e-folding time of 15.8 months, slightly longer than the 12–14 months estimated from satellite data (e.g. Baran et al., 1993). Modelled extinction in the tropical and NH mid-latitude lower stratosphere shows reasonably good agreement with SAGE V7 data in both the mid-visible and near infra-red. However, for the first six months after the eruption simulated AOD and SAD are larger (~ 2–4 times) than the satellite measurements, and the model enhancement in R_{eff} is too low (e.g. compared to Bauman et al., 2003). Lack of radiative coupling in these simulations likely explains the underestimate in the transport of the Pinatubo plume to the Southern Hemisphere in the model, and this may also have caused tropical AOD and SAD to be too high in the tropics.

To better understand how the particle size distribution was perturbed during the Pinatubo eruption, we have compared against mid-latitude balloon-borne measurements during that time period, allowing a strong observational constraint on concentrations of particles larger than 5, 150, 250, 550, 750 and 1000 nm. Although there have

[Title Page](#)[Abstract](#)[Introduction](#)[Conclusions](#)[References](#)[Tables](#)[Figures](#)[|◀](#)[▶|](#)[Back](#)[Close](#)[Full Screen / Esc](#)[Printer-friendly Version](#)[Interactive Discussion](#)

**Simulation of
Pinatubo aerosol in
a CCM**

S. S. Dhomse et al.

[Title Page](#)[Abstract](#)[Introduction](#)[Conclusions](#)[References](#)[Tables](#)[Figures](#)[|◀](#)[▶|](#)[◀](#)[▶](#)[Back](#)[Close](#)[Full Screen / Esc](#)[Printer-friendly Version](#)[Interactive Discussion](#)

been many model studies covering the Pinatubo period over the 22 yr since the eruption, to our knowledge, this is the first time the full profile of a simulated size distribution in a global model has been compared to these measurements in volcanically perturbed conditions.

- 5 In volcanically quiescent conditions, the model finds no nucleation occurring in the stratosphere, with particles forming mainly in the tropical upper troposphere. At NH mid-latitudes, the model agrees well with the observations, indicating that only a small proportion of these nucleated particles have grown to 150 nm by coagulation and condensation, with N_5 larger than N_{150} by around a factor of 10. We have investigated the
10 impact on the size distribution of the 20 Tg tropical injection of SO₂ from Pinatubo. Although the spatial and temporal evolution of the R_{eff} in the lower stratosphere seen by satellite is well captured by the model, the comparisons to the balloon measurements indicate that, at NH mid-latitudes, the model generates far too many particles in the size range 5–250 nm, although larger particle sizes compare well to the observations. The
15 high bias in N_{150} is consistent with the high biases seen in AOD and SAD in the initial phase of the eruption, and with the general low bias apparent in R_{eff} . These findings underline the importance of better constraining nucleation and growth of these finest particles in the first few months after the eruption to improve prediction of volcanic impacts on climate with stratospheric aerosol microphysics models.
- 20 **Acknowledgements.** We would like to thank P. B. Russell for effective radius data. This work was supported by the UK Natural Environment Research Council (NERC grants NE/E005659/1 and NE/E017150/1). GWM and KSC received funding from the National Centre for Atmospheric Science, one of the NERC research centres. GWM received EU funding from the European Research Council (ERC) under Seventh Framework Programme (FP7) consortium projects
25 MACC and MACC-II (grant agreements 218793 and 283576 respectively). NB, MD, CEJ, FOC were supported as part the UK Integrated Climate Programme funded by the Department for Energy and Climate Change (DECC) and Department for Environment Food and Rural Affairs – DECC/Defra (GA01101). We would also like to thank James Keeble for his help during model development. We acknowledge use of the MONSooN system, a collaborative facility supplied
30 under the Joint Weather and Climate Research Programme, which is a strategic partnership

between the UK Met Office and the Natural Environment Research Council. This work has been also supported by NIWA as part of its Government-funded, core research programme. The in situ measurements were supported by the US National Science Foundation. Current measurements are supported under grant number ATM-0437406.

5 References

- Andres, R. and Kasgnoc, A.: A time-averaged inventory of subaerial volcanic sulfur emissions, *J. Geophys. Res.-Atmos.*, 103, 25251–25261, 1998. 2807
- Andrews, D. G., Holton, J. R., and Leovy, C. B.: Middle atmosphere dynamics, Academic Press, New York, NY, USA, 1987. 2813
- Aquila, V., Oman, L. D., Stolarski, R. S., Colarco, P. R., and Newman, P. A.: Dispersion of the volcanic sulfate cloud from a Mount Pinatubo-like eruption, *J. Geophys. Res.-Atmos.*, 117, D06216, doi:10.1029/2011JD016968, 2012. 2804, 2805, 2819
- Arfeuille, F., Luo, B. P., Heckendorn, P., Weisenstein, D., Sheng, J. X., Rozanov, E., Schraner, M., Brönnimann, S., Thomason, L. W., and Peter, T.: Uncertainties in modelling the stratospheric warming following Mt. Pinatubo eruption, *Atmos. Chem. Phys. Discuss.*, 13, 4601–4635, doi:10.5194/acpd-13-4601-2013, 2013. 2804, 2815, 2850
- Arnold, F., Fabian, R., and Joos, W.: Measurements of the height variation of sulfuric acid vapor concentrations in the stratosphere, *Geophys. Res. Lett.*, 8, 293–296, 1981. 2826
- Ayers, G., Gillett, R., and Gras, J.: On the vapor pressure of sulfuric acid, *Geophys. Res. Lett.*, 7, 433–436, 1980. 2810
- Baldwin, M., Gray, L., Dunkerton, T., Hamilton, K., Haynes, P., Randel, W., Holton, J., Alexander, M., Hirota, I., and Horinouchi, T.: The quasi-biennial oscillation, *Rev. Geophys.*, 39, 179–229, 2001. 2813
- Baran, A. J. and Foot, J. S.: New application of the operational sounder HIRS in determining a climatology of sulphuric acid aerosol from the Pinatubo eruption, *J. Geophys. Res.-Atmos.*, 99, 25673–25679, 1994. 2804, 2817
- Baran, A. J., Foot, J. S., and Dibben, P. C.: Satellite detection of volcanic sulfuric-acid aerosol, *Geophys. Res. Lett.*, 20, 1799–1801, 1993. 2830

[Title Page](#)[Abstract](#)[Introduction](#)[Conclusions](#)[References](#)[Tables](#)[Figures](#)[◀](#)[▶](#)[Back](#)[Close](#)[Full Screen / Esc](#)[Printer-friendly Version](#)[Interactive Discussion](#)

Simulation of Pinatubo aerosol in a CCM

S. S. Dhomse et al.

[Title Page](#)

[Abstract](#)

[Introduction](#)

[Conclusions](#)

[References](#)

[Tables](#)

[Figures](#)

◀

▶

[Back](#)

[Close](#)

[Full Screen / Esc](#)

[Printer-friendly Version](#)

[Interactive Discussion](#)



- Bauman, J., Russell, P., Geller, M., and Hamill, P.: A stratospheric aerosol climatology from SAGE II and CLAES measurements: 2. Results and comparisons, 1984–1999, *J. Geophys. Res.*, 108, D134383, doi:10.1029/2002JD002993, 2003. 2805, 2823, 2830, 2851
- Bekki, S.: Oxidation of volcanic SO₂: a sink for stratospheric OH and H₂O, *Geophys. Res. Lett.*, 22, 913–916, 1995. 2817
- Bekki, S. and Pyle, J.: Two dimensional assessment of the impact of aircraft sulphur emissions on the stratospheric sulphate aerosol layer, *J. Geophys. Res.-Atmos.*, 97, 15839–15847, 1992. 2808
- Bekki, S., Law, K., and Pyle, J.: Effect of ozone depletion on atmospheric CH₄ and CO concentrations, *Nature*, 371, 595–597, 1994. 2804
- Bekki, S., Pyle, J. A., Zhong, W., Toumi, R., Haigh, J. D., and Pyle, D. M.: The role of microphysical and chemical processes in prolonging the climate forcing of the Toba eruption, *Geophys. Res. Lett.*, 23, 2669–2672, 1996. 2804
- Binkowski, F. S. and Roselle, S. J.: Models-3 Community Multiscale Air Quality (CMAQ) model aerosol component, 1. Model description, *J. Geophys. Res.-Atmos.*, 108, D64183, doi:10.1029/2001JD001409, 2003. 2811
- Bluth, G. J., Doiron, S. D., Schnetzler, C. C., Krueger, A. J., and Walter, L. S.: Global tracking of the SO₂ clouds from the June, 1991 Mount Pinatubo eruptions, *Geophys. Res. Lett.*, 19, 151–154, 1992. 2803, 2813, 2817
- Bluth, G. J. S., Rose, W. I., Sprod, I. E., and Krueger, A. J.: Stratospheric loading of sulfur from explosive volcanic eruptions, *J. Geol.*, 105, 671–683, 1997. 2817
- Braesicke, P., Keeble, J., Yang, X., Stiller, G., Kellmann, S., Abraham, N. L., Archibald, A., Telford, P., and Pyle, J. A.: Circulation anomalies in the Southern Hemisphere and ozone changes, *Atmos. Chem. Phys.*, 13, 10677–10688, doi:10.5194/acp-13-10677-2013, 2013. 2806
- Carslaw, K. and Kärcher, B.: Stratospheric aerosol processes. In: Thomason L. and Peter Th. (Eds.) SPARC Assessment of Stratospheric Aerosol Properties (ASAP), pp. 1–28, SPARC Report No. 4, World Climate Research Programme, 2006. 2807, 2811
- Carslaw, K. S., Luo, B., and Peter, T.: An analytic expression for the composition of aqueous HNO₃–H₂SO₄ stratospheric aerosols including gas phase removal of HNO₃, *Geophys. Res. Lett.*, 22, 1877–1880, 1995. 2809
- Carver, G. D., Brown, P. D., and Wild, O.: The ASAD atmospheric chemistry integration package and chemical reaction database, *Comput. Phys. Commun.*, 105, 197–215, 1997. 2807

- Chipperfield, M.: New version of the TOMCAT/SLIMCAT offline chemical transport model: inter-comparison of stratospheric tracer experiments, *Q. J. Roy. Meteor. Soc.*, 132, 1179–1203, 2006. 2808
- 5 Chipperfield, M. and Pyle, J.: Model sensitivity studies of Arctic ozone depletion, *J. Geophys. Res.-Atmos.*, 103, 28389–28403, 1998. 2807
- 10 Chipperfield, M. P., Liang, Q., Strahan, S. E., Morgenstern, O., Dhomse, S. S., Abraham, N. L., Archibald, A. T., S. Bekki, S., Braesicke, P., Di Genova, G., Fleming, E. L., Hardiman, S. C., Iachetti, D., Jackman, C. H., Kinnison, D. E., Marchand, M., Pitari, G., Pyle, J. A., Rozanov, E., Stenke, A., and Tummon, F.: Multi-model estimates of atmospheric lifetimes of long-lived ozone depleting substances: present and future, *J. Geophys. Res.*, accepted, 2014. 2814
- D'Almeida, G. A., Koepke, P., and Shettle, E. P.: Atmospheric aerosols: global climatology and radiative characteristics, *A. Deepak Pub. Hampton, Virginia, USA*, 1991. 2812
- 15 Damadeo, R. P., Zawodny, J. M., Thomason, L. W., and Iyer, N.: SAGE version 7.0 algorithm: application to SAGE II, *Atmos. Meas. Tech. Discuss.*, 6, 5101–5171, doi:10.5194/amtd-6-5101-2013, 2013. 2815
- 20 Dee, D. P., Uppala, S. M., Simmons, A. J., Berrisford, P., Poli, P., Kobayashi, S., Andrae, U., Balmaseda, M. A., Balsamo, G., Bauer, P., Bechtold, P., Beljaars, A. C. M., van de Berg, L., Bidlot, J., Bormann, N., Delsol, C., Dragani, R., Fuentes, M., Geer, A. J., Haimberger, L., Healy, S., Hersbach, H., Holm, E. V., Isaksen, L., Kallberg, P., Koehler, M., Matricardi, M., McNally, A. P., Monge-Sanz, B. M., Morcrette, J.-J., Peubey, C., de Rosnay, P., Tavolato, C., Thapaut, J.-N., and Vitart, F.: The ERA-Interim reanalysis: Configuration and performance of the data assimilation system, *Q. J. R. Meteor. Soc.*, 133, 1972–1990, 2011. 2813, 2844
- 25 Dentener, F., Kinne, S., Bond, T., Boucher, O., Cofala, J., Generoso, S., Ginoux, P., Gong, S., Hoelzemann, J. J., Ito, A., Marelli, L., Penner, J. E., Putaud, J.-P., Textor, C., Schulz, M., van der Werf, G. R., and Wilson, J.: Emissions of primary aerosol and precursor gases in the years 2000 and 1750 prescribed data-sets for AeroCom, *Atmos. Chem. Phys.*, 6, 4321–4344, doi:10.5194/acp-6-4321-2006, 2006. 2828
- 30 Deshler, T.: In situ measurements of Pinatubo aerosol over Kiruna on four days between 18 January and 13 February 1992, *Geophys. Res. Lett.*, 21, 1323–1326, 1994. 2804, 2805
- Deshler, T.: A review of global stratospheric aerosol: measurements, importance, life cycle, and local stratospheric aerosol, *Atmos. Res.*, 90, 223–232, 2008. 2814

[Title Page](#)

[Abstract](#)

[Introduction](#)

[Conclusions](#)

[References](#)

[Tables](#)

[Figures](#)

◀

▶

◀

▶

[Back](#)

[Close](#)

[Full Screen / Esc](#)

[Printer-friendly Version](#)

[Interactive Discussion](#)



Simulation of Pinatubo aerosol in a CCM

S. S. Dhomse et al.

[Title Page](#)

[Abstract](#)

[Introduction](#)

[Conclusions](#)

[References](#)

[Tables](#)

[Figures](#)

[◀](#)

[▶](#)

[Back](#)

[Close](#)

[Full Screen / Esc](#)

[Printer-friendly Version](#)

[Interactive Discussion](#)



Deshler, T., Hofmann, D., Johnson, B., and Rozier, W.: Balloonborne measurements of the Pinatubo aerosol size distribution and volatility at Laramie, Wyoming during the summer of 1991, *Geophys. Res. Lett.*, 19, 199–202, 1992. 2815, 2816, 2818, 2824

5 Deshler, T., Hervig, M. E., Hofmann, D. J., Rosen, J. M., and Liley, J. B.: Thirty years of in situ stratospheric aerosol size distribution measurements from Laramie, Wyoming (41 degrees N), using balloon-borne instruments, *J. Geophys. Res.-Atmos.*, 108, D54167, doi:10.1029/2002JD002514, 2003. 2802, 2811, 2815, 2816, 2824

10 Driscoll, S., Bozzo, A., Gray, L. J., Robock, A., and Stenchikov, G.: Coupled Model Intercomparison Project 5 (CMIP5) simulations of climate following volcanic eruptions, *J. Geophys. Res.-Atmos.*, 117, D17105, doi:10.1029/2012JD017607, 2012. 2803

English, J. M., Toon, O. B., and Mills, M. J.: Microphysical simulations of sulfur burdens from stratospheric sulfur geoengineering, *Atmos. Chem. Phys.*, 12, 4775–4793, doi:10.5194/acp-12-4775-2012, 2012. 2804

15 English, J. M., Toon, O. B., and Mills, M. J.: Microphysical simulations of large volcanic eruptions: Pinatubo and Toba, *J. Geophys. Res.-Atmos.*, 118, 1880–1895, doi:10.1002/jgrd.50196, 2013. 2804, 2805

Giauque, W., Hornung, E., Kunzler, J., and Rubin, T.: The thermodynamic properties of aqueous sulfuric acid solutions and hydrates from 15 to 300 K. 1, *J. Am. Chem. Soc.*, 82, 62–70, 1960. 2810

20 Graf, H. F., Kirchner, I., Robock, A., and Schult, I.: Pinatubo eruption winter climate effects: model versus observations, *Clim. Dynam.*, 9, 81–93, 1993. 2802

Hall, T. M., Waugh, D. W., Boering, K. A., and Plumb, R. A.: Evaluation of transport in stratospheric models, *J. Geophys. Res.-Atmos.*, 104, 18815–18839, 1999. 2814, 2844

25 Hamill, P., Jensen, E. J., Russell, P., and Bauman, J. J.: The life cycle of stratospheric aerosol particles, *B. Am. Meteorol. Soc.*, 78, 1395–1410, 1997. 2810, 2828

Hamill, P., Brogniez, C., Thomason, L., Deshler, T., Antuña, J., Baumgardner, D., Bevilacqua, R., Brock, C., David, C., Fussen, D., Hervig, M., Hostettler, C. A., Lee, S.-H., Mergenthaler, J., Osborn, M. T., Raga, G., Reeves, J. M., Rosen, J., and Wilson, J. C.: Instrument Descriptions, edited by: Thomason, L. and Peter, Th., SPARC Assessment of Stratospheric Aerosol Properties (ASAP), 77–106, SPARC Report No. 4, World Climate Research Programme, 2006. 2815, 2819, 2822, 2823

30 Hansen, J., Lacis, A., Ruedy, R., and Sato, M.: Potential climate impact of Mount Pinatubo eruption, *Geophys. Res. Lett.*, 19, 215–218, 1992. 2802

Simulation of
Pinatubo aerosol in
a CCM

S. S. Dhomse et al.

[Title Page](#)

[Abstract](#)

[Introduction](#)

[Conclusions](#)

[References](#)

[Tables](#)

[Figures](#)

◀

▶

[Back](#)

[Close](#)

[Full Screen / Esc](#)

[Printer-friendly Version](#)

[Interactive Discussion](#)



- Heintzenberg, J., Birmili, W., Wiedensohler, A., Nowak, A., and Tuch, T.: Structure, variability and persistence of the submicrometre marine aerosol, *Tellus B*, 56, 357–367, 2004. 2812
- Hewitt, H. T., Copsey, D., Culverwell, I. D., Harris, C. M., Hill, R. S. R., Keen, A. B., McLaren, A. J., and Hunke, E. C.: Design and implementation of the infrastructure of HadGEM3: the next-generation Met Office climate modelling system, *Geosci. Model Dev.*, 4, 223–253, doi:10.5194/gmd-4-223-2011, 2011. 2806
- Hommel, R., Timmreck, C., and Graf, H. F.: The global middle-atmosphere aerosol model MAECHAM5-SAM2: comparison with satellite and in-situ observations, *Geosci. Model Dev.*, 4, 809–834, doi:10.5194/gmd-4-809-2011, 2011. 2810, 2816, 2826
- Hurrell, J. W., Hack, J. J., Shea, D., Caron, J. M., and Rosinski, J.: A new sea surface temperature and sea ice boundary dataset for the Community Atmosphere Model, *J. Climate*, 21, 5145–5153, 2008. 2806
- Jones, C. D., Hughes, J. K., Bellouin, N., Hardiman, S. C., Jones, G. S., Knight, J., Lidlicoat, S., O'Connor, F. M., Andres, R. J., Bell, C., Boo, K.-O., Bozzo, A., Butchart, N., Cadule, P., Corbin, K. D., Doutriaux-Boucher, M., Friedlingstein, P., Gornall, J., Gray, L., Halloran, P. R., Hurt, G., Ingram, W. J., Lamarque, J.-F., Law, R. M., Meinshausen, M., Osprey, S., Palin, E. J., Parsons Chini, L., Raddatz, T., Sanderson, M. G., Sellar, A. A., Schurer, A., Valdes, P., Wood, N., Woodward, S., Yoshioka, M., and Zerroukat, M.: The HadGEM2-ES implementation of CMIP5 centennial simulations, *Geosci. Model Dev.*, 4, 543–570, doi:10.5194/gmd-4-543-2011, 2011. 2803
- Kerminen, V.-M., and Kulmala, M.: Analytical formulae connecting the “real” and the “apparent” nucleation rate and the nuclei number concentration for atmospheric nucleation events, *J. Aerosol Sci.*, 33, 609–622, 2002. 2811
- Kettle, A. and Andreae, M.: Flux of dimethylsulfide from the oceans: a comparison of updated data sets and flux models, *J. Geophys. Res.-Atmos.*, 105, 26793–26808, 2000. 2807
- Kokkola, H., Hommel, R., Kazil, J., Niemeier, U., Partanen, A.-I., Feichter, J., and Timmreck, C.: Aerosol microphysics modules in the framework of the ECHAM5 climate model – intercomparison under stratospheric conditions, *Geosci. Model Dev.*, 2, 97–112, doi:10.5194/gmd-2-97-2009, 2009. 2812
- Kreidenweis, S. M., Walcek, C. J., Feingold, G., Gong, W., Jacobson, M. Z., Kim, C.-H., Liu, X., Penner, J. E., Nenes, A., and Seinfeld, J. H.: Modification of aerosol mass and size distribution due to aqueous-phase SO₂ oxidation in clouds: Comparisons of several models, *Geophys. Res.-Atmos.*, 108, D74213, doi:10.1029/2002JD002697, 2003. 2843

Simulation of Pinatubo aerosol in a CCM

S. S. Dhomse et al.

[Title Page](#)

[Abstract](#)

[Introduction](#)

[Conclusions](#)

[References](#)

[Tables](#)

[Figures](#)

◀

▶

◀

▶

[Back](#)

[Close](#)

[Full Screen / Esc](#)

[Printer-friendly Version](#)

[Interactive Discussion](#)



- Kulmala, M. and Laaksonen, A.: Binary nucleation of water-sulfuric acid system: comparison of classical theories with different H_2SO_4 saturation vapor pressures, *J. Chem. Phys.*, 93, 696, 1990. 2810
- Kulmala, M., Laaksonen, A., and Pirjola, L.: Parameterizations for sulfuric acid/water nucleation rates, *J. Geophys. Res.-Atmos.*, 103, 8301–8307, 1998. 2810, 2811
- 5 Labitzke, K. and McCormick, M.: Stratospheric temperature increases due to Pinatubo aerosols, *Geophys. Res. Lett.*, 19, 207–210, 1992. 2802
- Lacis, A., Hansen, J., and Sato, M.: Climate forcing by stratospheric aerosols, *Geophys. Res. Lett.*, 19, 1607–1610, 1992. 2802
- 10 Lamarque, J.-F., Bond, T. C., Eyring, V., Granier, C., Heil, A., Klimont, Z., Lee, D., Liousse, C., Mieville, A., Owen, B., Schultz, M. G., Shindell, D., Smith, S. J., Stehfest, E., Van Aardenne, J., Cooper, O. R., Kainuma, M., Mahowald, N., McConnell, J. R., Naik, V., Riahi, K., and van Vuuren, D. P.: Historical (1850–2000) gridded anthropogenic and biomass burning emissions of reactive gases and aerosols: methodology and application, *Atmos. Chem. Phys.*, 10, 7017–7039, doi:10.5194/acp-10-7017-2010, 2010. 2807
- 15 Liss, P. S. and Merlivat, L.: Air–Sea Gas Exchange Rates: Introduction and Synthesis, Springer, the Netherlands, 113–127, 1986. 2807
- Mann, G. W., Carslaw, K. S., Spracklen, D. V., Ridley, D. A., Manktelow, P. T., Chipperfield, M. P., Pickering, S. J., and Johnson, C. E.: Description and evaluation of GLOMAP-mode: a modal global aerosol microphysics model for the UKCA composition-climate model, *Geosci. Model Dev.*, 3, 519–551, doi:10.5194/gmd-3-519-2010, 2010. 2806, 2808, 2809, 2810, 2812
- 20 Mann, G. W., Carslaw, K. S., Ridley, D. A., Spracklen, D. V., Pringle, K. J., Merikanto, J., Korhonen, H., Schwarz, J. P., Lee, L. A., Manktelow, P. T., Woodhouse, M. T., Schmidt, A., Breider, T. J., Emmerson, K. M., Reddington, C. L., Chipperfield, M. P., and Pickering, S. J.: Intercomparison of modal and sectional aerosol microphysics representations within the same 3-D global chemical transport model, *Atmos. Chem. Phys.*, 12, 4449–4476, doi:10.5194/acp-12-4449-2012, 2012. 2808, 2812
- 25 Martin, E., George, C., and Mirabel, P.: Densities and surface tensions of $H_2SO_4/HNO_3/H_2O$ solutions, *Geophys. Res. Lett.*, 27, 197–200, 2000. 2809
- Mccormick, M. and Veiga, R.: SAGE II measurements of early Pinatubo aerosols, *Geophys. Res. Lett.*, 19, 155–158, 1992. 2804, 2814, 2817
- 30 McCormick, M. P., Thomason, L. W., and Trepte, C. R.: Atmospheric effects of the Mt. Pinatubo eruption, *Nature*, 373, 399–404, 1995. 2802, 2819

- Mills, M. J., Toon, O. B., Vaida, V., Hintze, P. E., Kjaergaard, H. G., Schofield, D. P., and Robinson, T. W.: Photolysis of sulfuric acid vapor by visible light as a source of the polar stratospheric CN layer, *J. Geophys. Res.-Atmos.*, 110, D08201, doi:10.1029/2004JD005519D8, 2005. 2807
- 5 Montzka, S., Calvert, P., Hall, B., Elkins, J., Conway, T., Tans, P., and Sweeney, C.: On the global distribution, seasonality, and budget of atmospheric carbonyl sulfide (COS) and some similarities to CO₂, *J. Geophys. Res.-Atmos.*, 112, D09302, doi:10.1029/2006JD007665, 2007. 2807
- 10 Morgenstern, O., Braesicke, P., O'Connor, F. M., Bushell, A. C., Johnson, C. E., Osprey, S. M., and Pyle, J. A.: Evaluation of the new UKCA climate-composition model – Part 1: The stratosphere, *Geosci. Model Dev.*, 2, 43–57, doi:10.5194/gmd-2-43-2009, 2009. 2806, 2807
- 15 Morgenstern, O., Giorgetta, M. A., Shibata, K., Eyring, V., Waugh, D. W., Shepherd, T. G., Akiyoshi, H., Austin, J., Baumgaertner, A. J. G., Bekki, S., Braesicke, P., Bruehl, C., Chipperfield, M. P., Cugnet, D., Dameris, M., Dhomse, S., Frith, S. M., Garny, H., Gettelman, A., Hardiman, S. C., Hegglin, M. I., Joeckel, P., Kinnison, D. E., Lamarque, J. F., Mancini, E., Manzini, E., Marchand, M., Michou, M., Nakamura, T., Nielsen, J. E., Olivie, D., Pitari, G., Plummer, D. A., Rozanov, E., Scinocca, J. F., Smale, D., Teyssedre, H., Toohey, M., Tian, W., and Yamashita, Y.: Review of the formulation of present-generation stratospheric chemistry-climate models and associated external forcings, *J. Geophys. Res.-Atmos.*, 115, 2156–2202, 2010. 2807
- 20 Neu, J. L., Prather, M. J., and Penner, J. E.: Global atmospheric chemistry: integrating over fractional cloud cover, *J. Geophys. Res.-Atmos.*, 112, D11306, doi:10.1029/2006JD008007, 2007. 2808
- 25 Niemeier, U., Timmreck, C., Graf, H.-F., Kinne, S., Rast, S., and Self, S.: Initial fate of fine ash and sulfur from large volcanic eruptions, *Atmos. Chem. Phys.*, 9, 9043–9057, doi:10.5194/acp-9-9043-2009, 2009. 2812
- 30 Oman, L., Robock, A., Stenchikov, G. L., Thordarson, T., Koch, D., Shindell, D. T., and Gao, C. C.: Modeling the distribution of the volcanic aerosol cloud from the 1783–1784 Laki eruption, *J. Geophys. Res.-Atmos.*, 111, D12209, doi:10.1029/2005JD006899, 2006. 2804, 2809, 2817
- Pitari, G. and Mancini, E.: Short-term climatic impact of the 1991 volcanic eruption of Mt. Pinatubo and effects on atmospheric tracers, *Nat. Hazards Earth Syst. Sci.*, 2, 91–108, doi:10.5194/nhess-2-91-2002, 2002. 2805

Title Page	
Abstract	Introduction
Conclusions	References
Tables	Figures
	
	
Back	Close
Full Screen / Esc	
Printer-friendly Version	
Interactive Discussion	



Simulation of
Pinatubo aerosol in
a CCM

S. S. Dhomse et al.

[Title Page](#)

[Abstract](#)

[Introduction](#)

[Conclusions](#)

[References](#)

[Tables](#)

[Figures](#)

◀

▶

[Back](#)

[Close](#)

[Full Screen / Esc](#)

[Printer-friendly Version](#)

[Interactive Discussion](#)



- Reeves, J., Wilson, J., Brock, C., and Bui, T.: Comparison of aerosol extinction coefficients, surface area density, and volume density from SAGE II and in situ aircraft measurements, *J. Geophys. Res.-Atmos.*, 113, D10202, doi:10.1029/2007JD009357113, 2008. 2822
- Robock, A.: Volcanic eruptions and climate, *Rev. Geophys.*, 38, 191–219, 2000. 2802
- 5 Robock, A. and Mao, J.: Winter warming from large volcanic eruptions, *Geophys. Res. Lett.*, 19, 2405–2408, 1992. 2802
- Russell, P., Livingston, J., Pueschel, R., Bauman, J., Pollack, J., Brooks, S., Hamill, P., Thomason, L., Stowe, L., and Deshler, T.: Global to microscale evolution of the Pinatubo volcanic aerosol derived from diverse measurements and analyses, *J. Geophys. Res.*, 101, 18745–18763, 1996. 2805, 2822
- 10 Sander, S., Friedl, R., Golden, D., Kurylo, M., Huie, R., Orkin, V., Moortgat, G., Wine, P., Ravishankara, A., Kolb, C., Molina, M., Finlayson-Pitts, B., Huie, R., Orkin, V. L., and Keller-Rudek, H.: Chemical kinetics and photochemical data for use in atmospheric studies, NASA Panel for Data Evaluation, Evaluation number 15, JPL Publication 06-2, Vol. 4915, Jet Propulsion Laboratory, California Institute of Technology, Pasadena, California, 2006. 2807, 2843
- 15 Sato, M., Hansen, J. E., McCormick, M. P., and Pollack, J. B.: Stratospheric aerosol optical depths, 1850–1990, *J. Geophys. Res.-Atmos.*, 98, 22987–22994, 1993. 2803
- Scaife, A. A., Spangehl, T., Fereday, D. R., Cubasch, U., Langematz, U., Akiyoshi, H., Bekki, S., Braesicke, P., Butchart, N., and Chipperfield, M. P.: Climate change projections and stratosphere-troposphere interaction, *Clim. Dynam.*, 38, 2089–2097, 2012. 2802
- 20 Solomon, S., Portmann, R. W., Garcia, R. R., Thomason, L. W., Poole, L. R., and McCormick, M. P.: The role of aerosol variations in anthropogenic ozone depletion at northern midlatitudes, *J. Geophys. Res.-Atmos.*, 101, 6713–6727, 1996. 2802
- SPARC: SPARC Assessment of stratospheric aerosol properties (ASAP) SPARC Report No. 4, World Clim. Res. Programme, WCRP-124, WMO/TD-No.1295, 2006. 2807, 2815, 2821, 25 2850
- SPARC: SPARC Report on the Evaluation of Chemistry-Climate Models, World Clim. Res. Programme, WCRP-132, WMO/TD-No.1526, 2010. 2803, 2806
- SPARC: Lifetime of halogen source gases WMO Ozone Research and Monitoring Project Report No. 6, World Clim. Res. Programme, WCRP-113, WMO/TD-No.XXXX, 2013. 2813
- 30 Spracklen, D. V., Pringle, K. J., Carslaw, K. S., Chipperfield, M. P., and Mann, G. W.: A global off-line model of size-resolved aerosol microphysics: I. Model development and prediction

Simulation of Pinatubo aerosol in a CCM

S. S. Dhomse et al.

[Title Page](#)

[Abstract](#)

[Introduction](#)

[Conclusions](#)

[References](#)

[Tables](#)

[Figures](#)

◀

▶

[Back](#)

[Close](#)

[Full Screen / Esc](#)

[Printer-friendly Version](#)

[Interactive Discussion](#)



- of aerosol properties, *Atmos. Chem. Phys.*, 5, 2227–2252, doi:10.5194/acp-5-2227-2005, 2005. 2808
- Stenchikov, G. L., Kirchner, I., Robock, A., Graf, H., Antuna, J. C., Grainger, R., Lambert, A., and Thomason, L.: Radiative forcing from the 1991 Mount Pinatubo volcanic eruption, *J. Geophys. Res.-Atmos.*, 103, 13837–13857, 1998. 2803, 2809
- 5 Stier, P., Feichter, J., Kinne, S., Kloster, S., Vignati, E., Wilson, J., Ganzeveld, L., Tegen, I., Werner, M., Balkanski, Y., Schulz, M., Boucher, O., Minikin, A., and Petzold, A.: The aerosol-climate model ECHAM5-HAM, *Atmos. Chem. Phys.*, 5, 1125–1156, doi:10.5194/acp-5-1125-2005, 2005. 2808
- 10 Stokes, R. and Robinson, R.: Interactions in aqueous nonelectrolyte solutions. I. Solute-solvent equilibria, *J. Phys. Chem.*, 70, 2126–2131, 1966. 2809
- Strahan, S. E., Douglass, A. R., Stolarski, R. S., Akiyoshi, H., Bekki, S., Braesicke, P., Butchart, N., Chipperfield, M. P., Cugnet, D., Dhomse, S., Frith, S. M., Gettelman, A., Hardiman, S. C., Kinnison, D. E., Lamarque, J. F., Mancini, E., Marchand, M., Michou, M., Morgenstern, O., Nakamura, T., Olivie, D., Pawson, S., Pitari, G., Plummer, D. A., Pyle, J. A., Scinocca, J. F., Shepherd, T. G., Shibata, K., Smale, D., Teyssedre, H., Tian, W., and Yamashita, Y.: Using transport diagnostics to understand chemistry climate model ozone simulations, *J. Geophys. Res.-Atmos.*, 116, D17302, doi:10.1029/2010JD015360, 2011. 2814
- Taylor, K. E., Stouffer, R. J., and Meehl, G. A.: An overview of CMIP5 and the experiment design, *B. Am. Meteorol. Soc.*, 93, 485–498, 2012. 2803
- Telford, P., Braesicke, P., Morgenstern, O., and Pyle, J.: Reassessment of causes of ozone column variability following the eruption of Mount Pinatubo using a nudged CCM, *Atmos. Chem. Phys.*, 9, 4251–4260, doi:10.5194/acp-9-4251-2009, 2009. 2806
- Telford, P. J., Abraham, N. L., Archibald, A. T., Braesicke, P., Dalvi, M., Morgenstern, O., O'Connor, F. M., Richards, N. A. D., and Pyle, J. A.: Implementation of the Fast-JX Photolysis scheme (v6.4) into the UKCA component of the MetUM chemistry-climate model (v7.3), *Geosci. Model Dev.*, 6, 161–177, doi:10.5194/gmd-6-161-2013, 2013. 2806, 2808
- 25 Textor, C., Schulz, M., Guibert, S., Kinne, S., Balkanski, Y., Bauer, S., Berntsen, T., Berglen, T., Boucher, O., Chin, M., Dentener, F., Diehl, T., Easter, R., Feichter, H., Fillmore, D., Ghan, S., Ginoux, P., Gong, S., Grini, A., Hendricks, J., Horowitz, L., Huang, P., Isaksen, I., Iversen, I., Kloster, S., Koch, D., Kirkevåg, A., Kristjansson, J. E., Krol, M., Lauer, A., Lamarque, J. F., Liu, X., Montanaro, V., Myhre, G., Penner, J., Pitari, G., Reddy, S., Selander, Ø., Stier, P., Takemura, T., and Tie, X.: Analysis and quantification of the diversities of aerosol life cycles
- 30

Simulation of Pinatubo aerosol in a CCM

S. S. Dhomse et al.

[Title Page](#)[Abstract](#)[Introduction](#)[Conclusions](#)[References](#)[Tables](#)[Figures](#)[◀](#)[▶](#)[Back](#)[Close](#)[Full Screen / Esc](#)[Printer-friendly Version](#)[Interactive Discussion](#)

- within AeroCom, *Atmos. Chem. Phys.*, 6, 1777–1813, doi:10.5194/acp-6-1777-2006, 2006.
2816
- Thomason, L., Poole, L., and Deshler, T.: A global climatology of stratospheric aerosol surface area density deduced from Stratospheric Aerosol and Gas Experiment II measurements
5 1984–1994, *J. Geophys. Res.-Atmos.*, 102, 8967–8976, 1997. 2815
- Timmreck, C.: Three-dimensional simulation of stratospheric background aerosol: first results of a multiannual general circulation model simulation, *J. Geophys. Res.-Atmos.*, 106, 28313–
10 28332, 2001. 2804
- Timmreck, C., Graf, H.-F., and Feichter, J.: Simulation of Mt. Pinatubo volcanic aerosol with the Hamburg climate model ECHAM4, *Theor. Appl. Climatol.*, 62, 85–108, 1999. 2804, 2805,
2813
- Toohey, M., Krüger, K., Niemeier, U., and Timmreck, C.: The influence of eruption season on the global aerosol evolution and radiative impact of tropical volcanic eruptions, *Atmos. Chem. Phys.*, 11, 12351–12367, doi:10.5194/acp-11-12351-2011, 2011. 2804
- Trepte, C. R. and Hitchman, M. H.: Tropical stratospheric circulation deduced from satellite aerosol data, *Nature*, 355, 626–628, 1992. 2813
- Vehkamäki, H., Kulmala, M., Napari, I., Lehtinen, K. E., Timmreck, C., Noppel, M., and Laaksonen, A.: An improved parameterization for sulfuric acid–water nucleation rates for tropospheric and stratospheric conditions, *J. Geophys. Res.*, 107, D224622,
20 doi:10.1029/2002JD002184, 2002. 2811, 2828
- Vignati, E., Wilson, J., and Stier, P.: M7: an efficient size Resolved aerosol microphysics module for large scale aerosol transport models, *J. Geophys. Res.-Atmos.*, 109, D22202,
20 doi:10.1029/2003JD004485, 2004. 2812
- Weisenstein, D., Bekki, S., Mills, M., Pitari, G., and Timmreck, C.: Modeling of stratospheric aerosols, edited by: Thomasson, L. and Peter, Th., SPARC Assessment of Stratospheric Aerosol Properties (ASAP), 219–272, SPARC Report No. 4, World Climate Research Programme, 2006. 2820, 2821
- Weisenstein, D. K., Yue, G. K., Ko, M. K. W., Sze, N. D., Rodriguez, J. M., and Scott, C. J.: A two-dimensional model of sulfur species and aerosols, *J. Geophys. Res.-Atmos.*, 102, 13019–13035, 1997. 2804, 2807, 2843
- Wild, O., Zhu, X., and Prather, M. J.: Fast-J: Accurate simulation of in-and below-cloud photolysis in tropospheric chemical models, *J. Atmos. Chem.*, 37, 245–282, 2000. 2808

- Wilson, J., Cuvelier, C., and Raes, F.: A modeling study of global mixed aerosol fields, *J. Geophys. Res.-Atmos.*, 106, 34081–34108, 2001. 2812

WMO: Scientific Assessment of Ozone Depletion: 2010, Global Ozone Research and Monitoring Project Report 52, World Meteorological Organization, Geneva, 2011. 2806

Young, R. E., Houben, H., and Toon, O. B.: Radiatively forced dispersion of the Mt. Pinatubo volcanic cloud and induced temperature perturbations in the stratosphere during the first few months following the eruption, *Geophys. Res. Lett.*, 21, 369–372, 1994. 2802, 2813, 2821

Zdanovskii, A.: New methods for calculating solubilities of electrolytes in multicomponent systems, *Zh. Fiz. Khim.*, 22, 1475–1485, 1948. 2809



Simulation of Pinatubo aerosol in a CCM

S. S. Dhomse et al.

[Title Page](#)

[Abstract](#)

[Introduction](#)

[Conclusions](#)

[References](#)

[Tables](#)

[Figures](#)

[◀](#)

[▶](#)

[◀](#)

[▶](#)

[Back](#)

[Close](#)

[Full Screen / Esc](#)

[Printer-friendly Version](#)

[Interactive Discussion](#)



Table 1. Additional sulphur chemistry reactions and rates within UKCA, W = Weisenstein et al. (1997), JPL = Sander et al. (2006), K03 = Kreidenweis et al. (2003)

	Rate	Reference
DMS + O(³ P) → SO ₂	$1.3 \times 10^{-11} \exp(410/T)$	W, JPL
DMS + OH → SO ₂	$1.2 \times 10^{-11} \exp(-260/T)$	W
DMS + OH → MSA + SO ₂	$3.04 \times 10^{-12} \exp(350/T) \cdot (\gamma/1+\gamma)$ $\gamma = 5.53 \times 10^{-31} \exp(7460/T) \times [O_2]$	W
DMS + NO ₃ → SO ₂	$1.9 \times 10^{-13} \exp(500/T)$	W
OCS + O(³ P) → CO + SO ₂	$2.1 \times 10^{-11} \exp(-2200/T)$	W, JPL
OCS + OH → CO ₂ + SO ₂	$1.1 \times 10^{-13} \exp(-1200/T)$	W, JPL
SO ₂ + OH + M → SO ₃ + HO ₂	$k(T) = \frac{A}{1+B} \times 0.6^{(1+(\log B)^2)^{-1}}$ $A = 3.0 \times 10^{-31} \times (300/T)^{3.3}$ $B = A/1.5 \times 10^{-12}$	W
SO ₂ + O ₃ → SO ₃	$3.0 \times 10^{-12} \exp(-7000/T)$	W, JPL
SO ₃ + H ₂ O → H ₂ SO ₄	$8.5 \times 10^{-41} \exp(6540/T) \cdot [H_2O]$	JPL
SO ₂ + H ₂ O ₂ ^{aqueous} → SO ₄		K03
OCS + hν → CO + SO ₂	Photolysis	W
H ₂ SO ₄ + hν → SO ₃ + OH	Photolysis	W
SO ₃ + hν → SO ₂ + O(³ P)	Photolysis	W

Simulation of Pinatubo aerosol in a CCM

S. S. Dhomse et al.

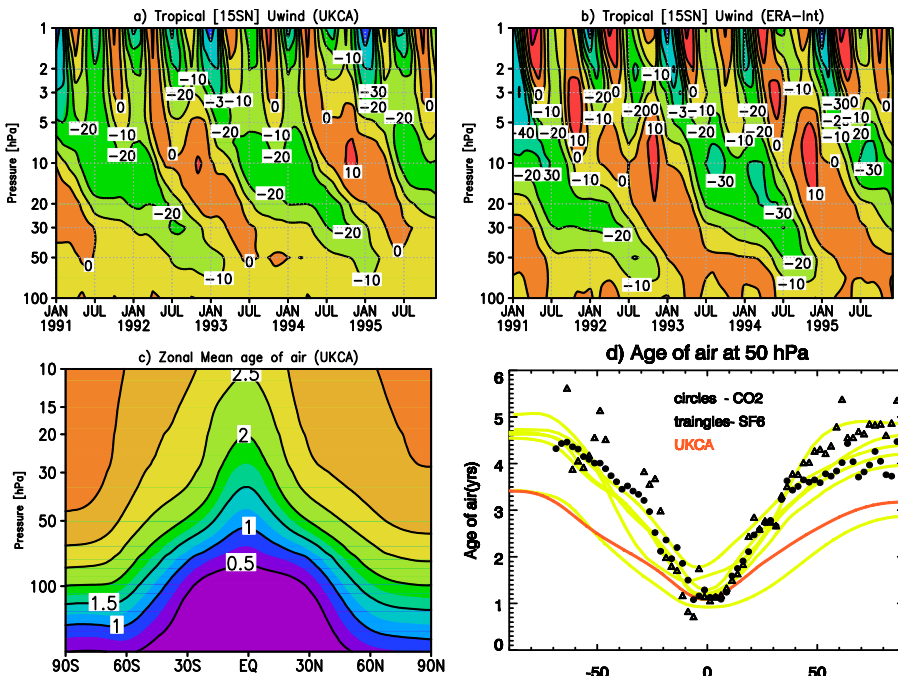


Fig. 1. (a) Model simulated tropical (15° S– 15° N) mean monthly mean zonal wind (m s^{-1} , QBO propagation). (b) Same as (a) but using ERA-interim reanalysis data (Dee et al., 2011). (c) Zonal mean age of air (years, mean 1991–2000), and (d) mean age of air (1991–2000) comparison at 50 hPa. Traingle and filled circles show estimated age of air from CO₂ and SF₆ (Hall et al., 1999). Mean age of air from various CCMs which participated in CCMVal lifetime assessment are shown with yellow lines and one from this study is shown with the red line.

- [Title Page](#)
- [Abstract](#) [Introduction](#)
- [Conclusions](#) [References](#)
- [Tables](#) [Figures](#)
- [◀](#) [▶](#)
- [◀](#) [▶](#)
- [Back](#) [Close](#)
- [Full Screen / Esc](#)
- [Printer-friendly Version](#)
- [Interactive Discussion](#)



Fig. 2. Time series of the global burden (in Tg of sulphur) of SO_2 (red), total sulphur (includes both SO_2 and aerosol, black), aerosol sulphur (dark blue) and aerosol sulphur in the upper troposphere and stratosphere (green) and lower and mid-troposphere (aqua), determined by above or below 400 hPa, for the simulations with (solid lines) and without (dashed lines) the Pinatubo eruption.

Simulation of Pinatubo aerosol in a CCM

S. S. Dhomse et al.

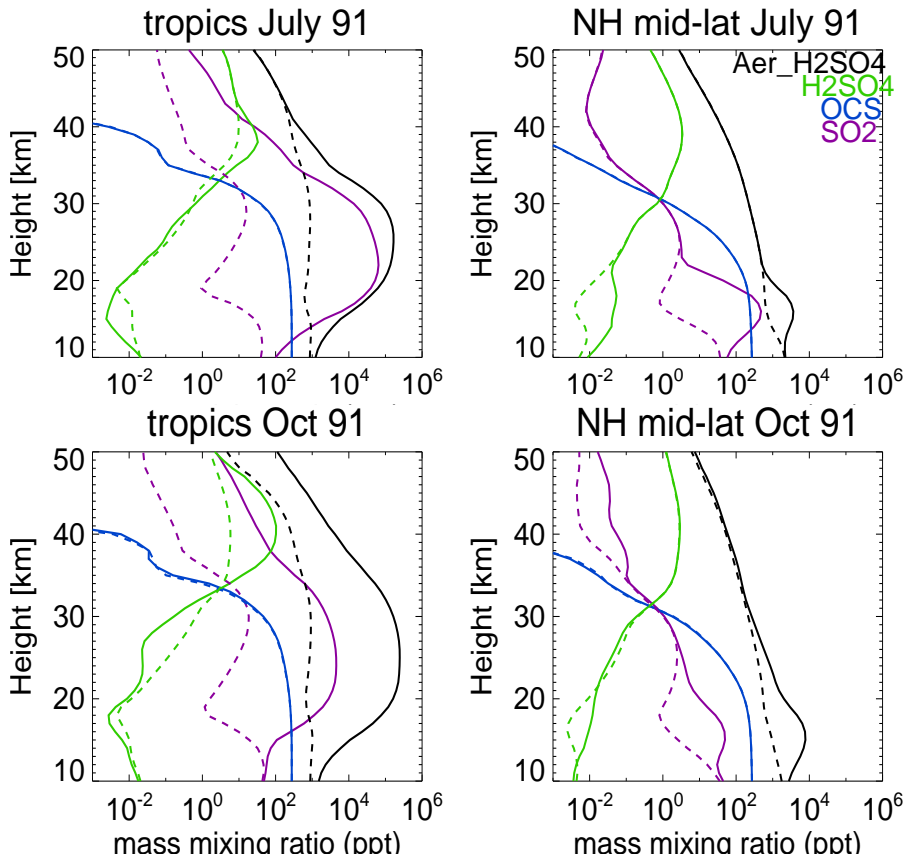


Fig. 3. Mixing ratios of various sulphur containing species (pptv) in the tropics (15° S–15° N, left) and NH mid-latitudes (35–60° N, right) during July 1991 (top) and October 1991 (bottom). Gas-phase and particle phase H₂SO₄ ratios are shown with black and green lines, respectively. OCS and SO₂ are shown with blue and green lines, respectively. Mixing ratios from the simulations with and without Pinatubo eruption are shown with solid and dashed lines, respectively.

Simulation of Pinatubo aerosol in a CCM

S. S. Dhomse et al.

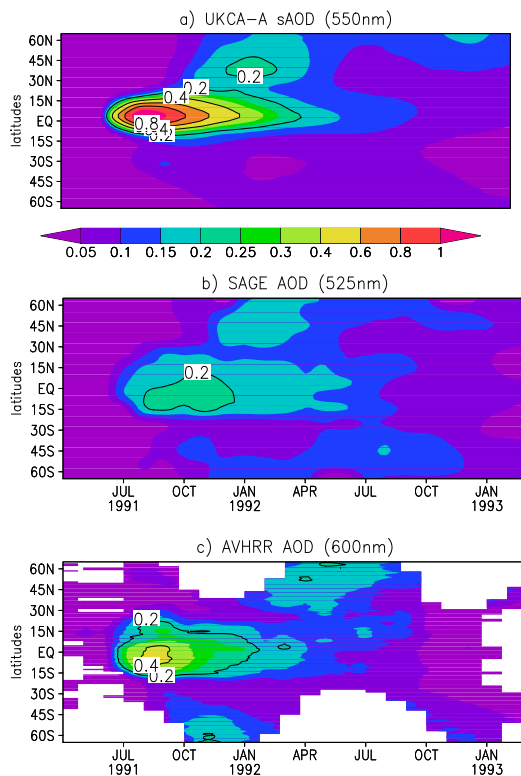


Fig. 4. Time series of model simulated zonal mean (**a**) stratosphere-only (integrated from the tropopause to top of the atmosphere) aerosol optical depth (AOD) derived using 525 nm extinctions. (**b**) and (**c**) are the AOD derived using SAGE II (525 nm) and AVHRR (600 nm) measurements. Due to the different viewing geometry of the AVHRR instrument (nadir viewing) AVHRR AOD shown (**c**) are after removal of background tropospheric AOD (22 months before the eruption).

Simulation of Pinatubo aerosol in a CCM

S. S. Dhomse et al.

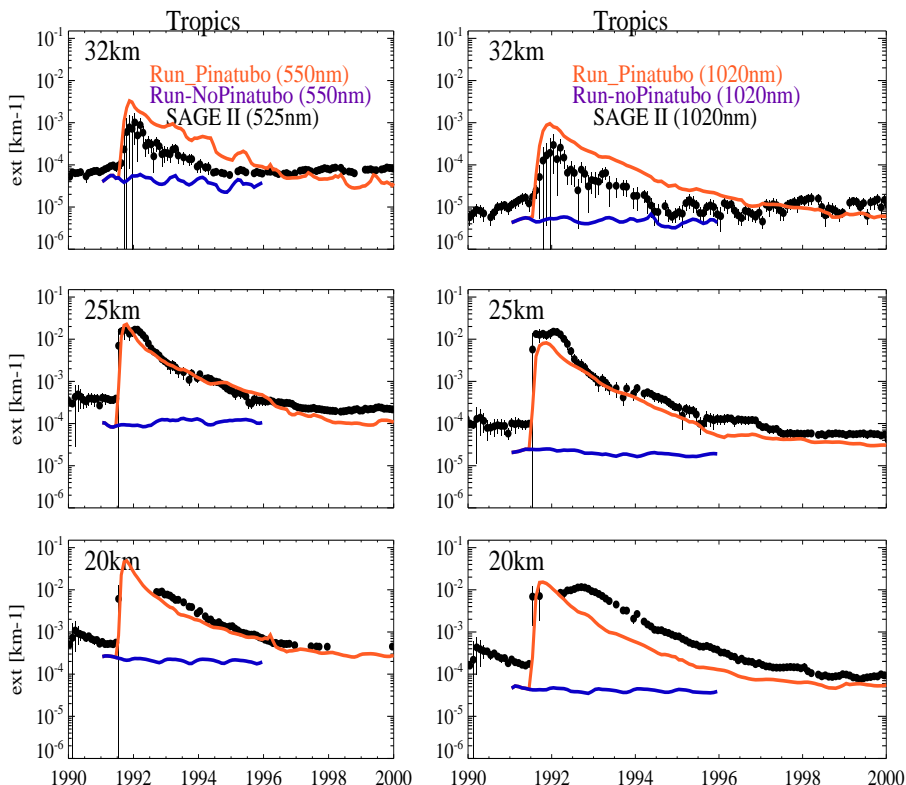


Fig. 5. Comparison between modelled and SAGE II (V7.0) retrieved extinction at 525 nm (left) and 1020 nm (right) in tropics (20° S– 20° N) for 20 km (bottom), 25 km (middle) and 35 km (top).

- [Title Page](#)
- [Abstract](#) [Introduction](#)
- [Conclusions](#) [References](#)
- [Tables](#) [Figures](#)
- [◀](#) [▶](#)
- [◀](#) [▶](#)
- [Back](#) [Close](#)
- [Full Screen / Esc](#)
- [Printer-friendly Version](#)
- [Interactive Discussion](#)



Simulation of Pinatubo aerosol in a CCM

S. S. Dhomse et al.

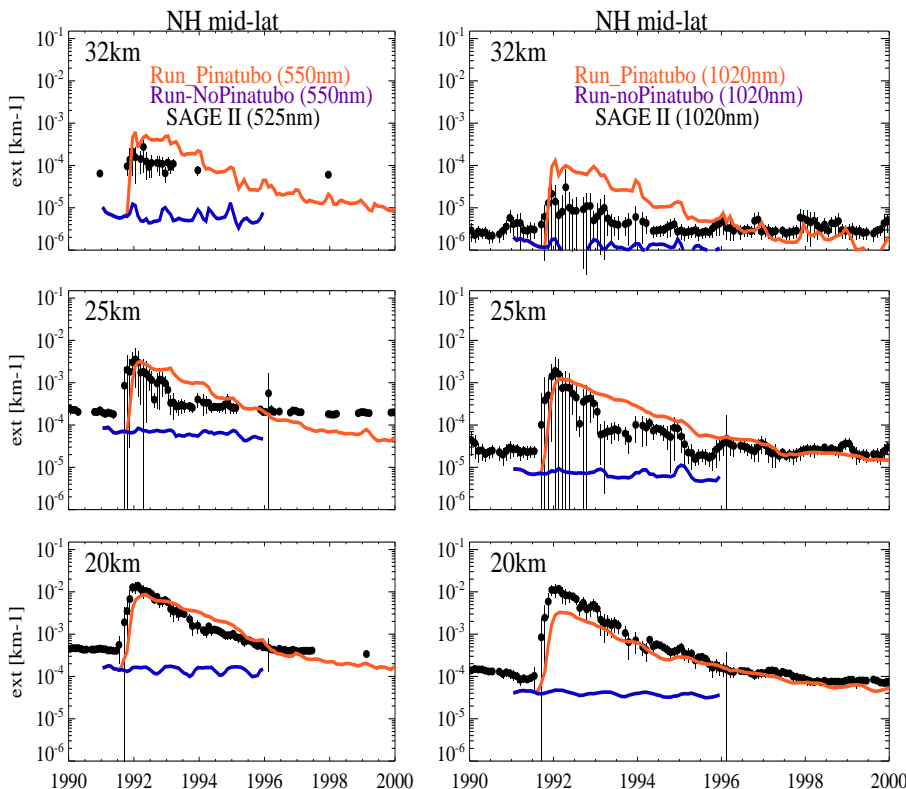


Fig. 6. Same as Fig. 5 but for NH mid-latitude (35–65° N).

Title Page

Abstract

Introduction

Conclusion

References

Tables

Figures



Back

Close

Full Screen / Esc

Interactive Discussion



Simulation of Pinatubo aerosol in a CCM

S. S. Dhomse et al.

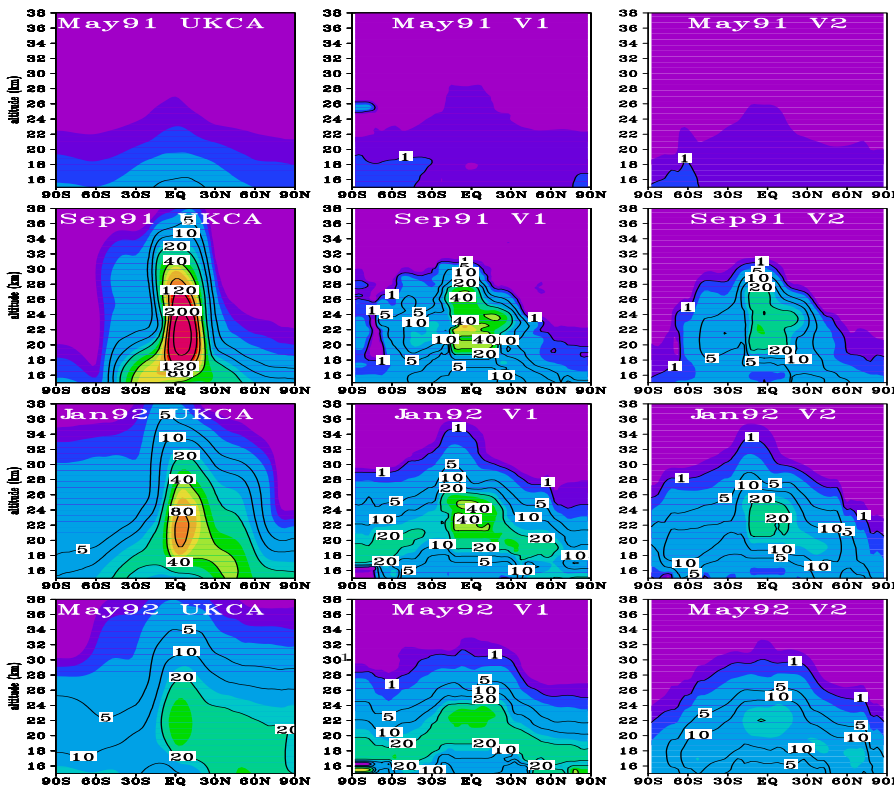


Fig. 7. Comparison between zonal mean modelled and satellite derived V1 and V2 SAD ($\mu\text{m}^2\text{cm}^{-3}$) from SPARC (2006) and Arfeuille et al. (2013), respectively, for various months before and after the eruption.

Printer-friendly Version

Interactive Discussion

|◀|▶|◀|▶|Back|Close|Full Screen / Esc

Title Page
Abstract
Conclusions
Tables

Introduction
References
Figures

**Simulation of
Pinatubo aerosol in
a CCM**

S. S. Dhomse et al.

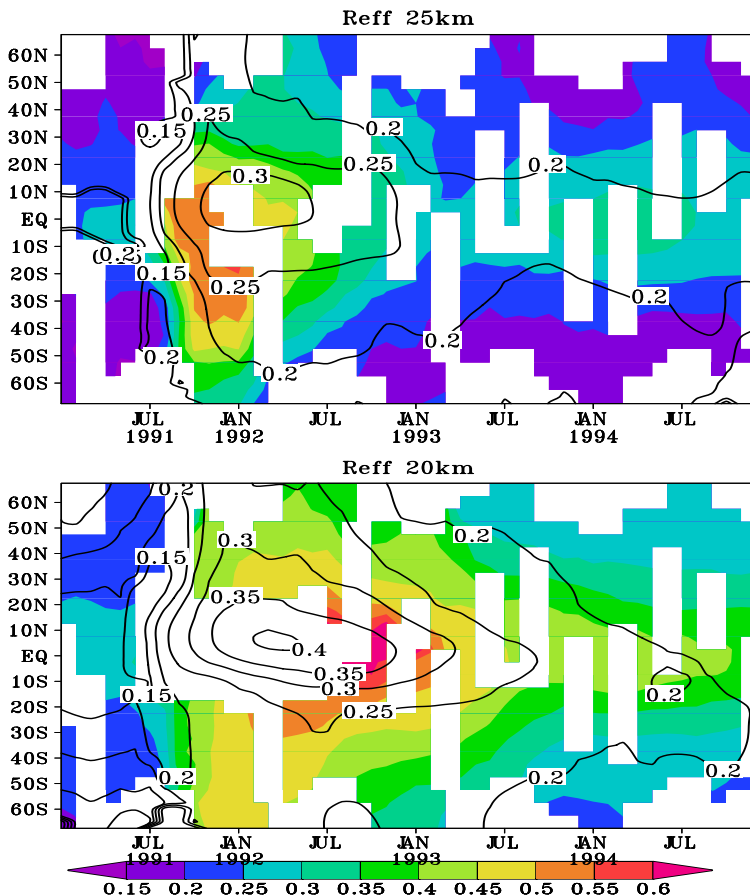


Fig. 8. Satellite derived (shaded, from Bauman et al., 2003) and modelled (contours) effective radius (μm) at 25 and 20 km.

- [Title Page](#)
- [Abstract](#) [Introduction](#)
- [Conclusions](#) [References](#)
- [Tables](#) [Figures](#)
- [◀](#) [▶](#)
- [◀](#) [▶](#)
- [Back](#) [Close](#)
- [Full Screen / Esc](#)
- [Printer-friendly Version](#)
- [Interactive Discussion](#)

Simulation of Pinatubo aerosol in a CCM

S. S. Dhomse et al.

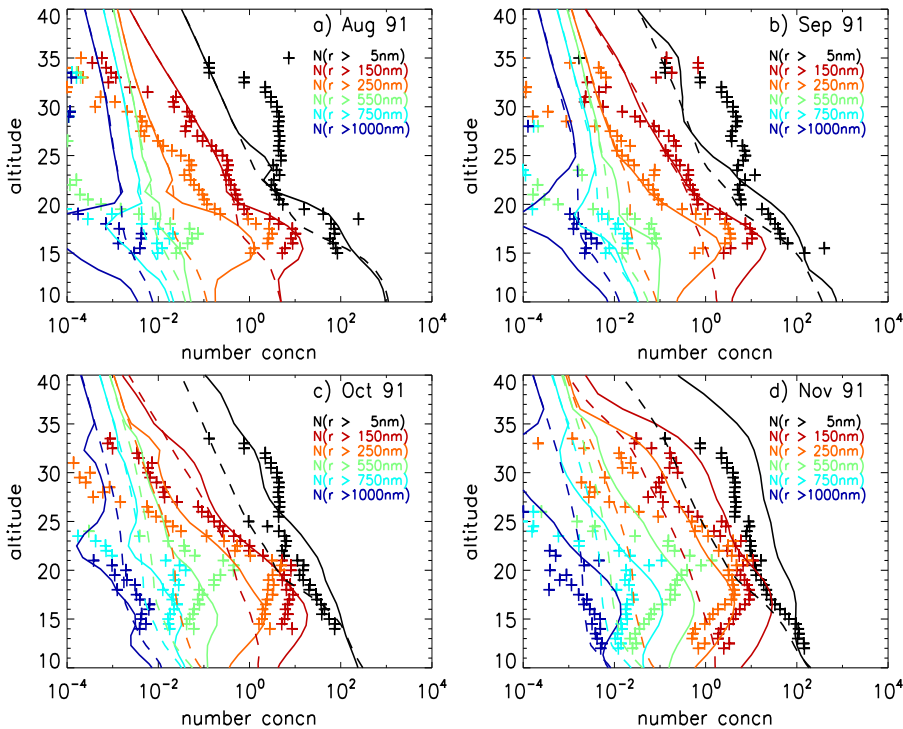


Fig. 9. August, September, October, November profiles of size-resolved number concentrations of particles (cm^{-3}) with radii larger than 5, 150, 250, 550, 750 and 1000 nm from Laramie (41.3°N , 105.5°W) are shown with plus (+) symbol. Solid and dashed lines show aerosol profiles from the Pinatubo and no-Pinatubo runs, respectively highlighting the region where model predicts the perturbation in the aerosol profiles.

Simulation of Pinatubo aerosol in a CCM

S. S. Dhomse et al.

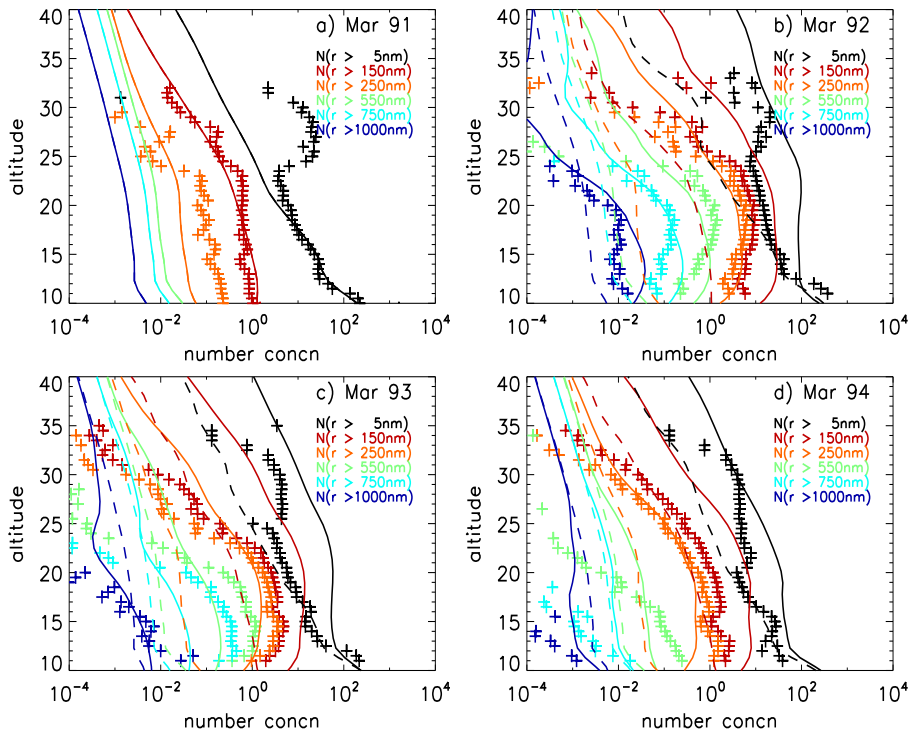


Fig. 10. Same as Fig. 9 but for March 1991, March 1992, March 1993 and March 1994.

[Title Page](#)

[Abstract](#)

[Introduction](#)

[Conclusions](#)

[References](#)

[Tables](#)

[Figures](#)

[|◀](#)

[▶|](#)

[◀](#)

[▶](#)

[Back](#)

[Close](#)

[Full Screen / Esc](#)

[Printer-friendly Version](#)

[Interactive Discussion](#)

Simulation of Pinatubo aerosol in a CCM

S. S. Dhomse et al.

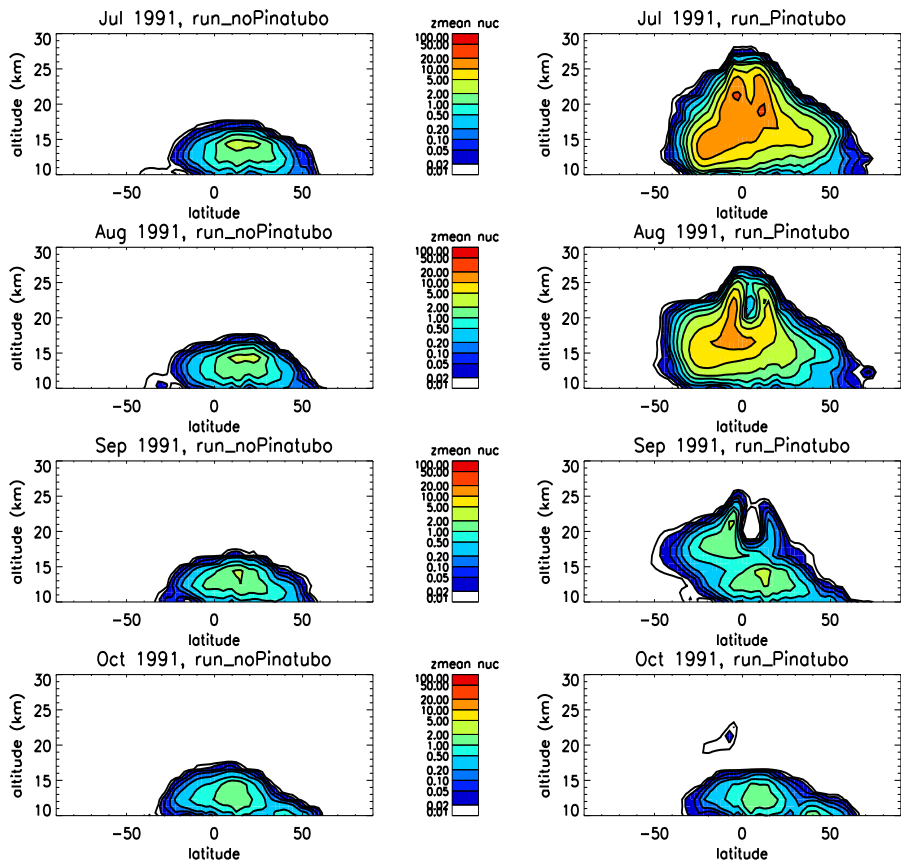


Fig. 11. Modelled nucleation rates ($\text{cm}^3 \text{s}^{-1}$) from non-Pinatubo (left) and Pinatubo (right) runs for (top to bottom) July, August, September and October 1991.

Simulation of Pinatubo aerosol in a CCM

S. S. Dhomse et al.

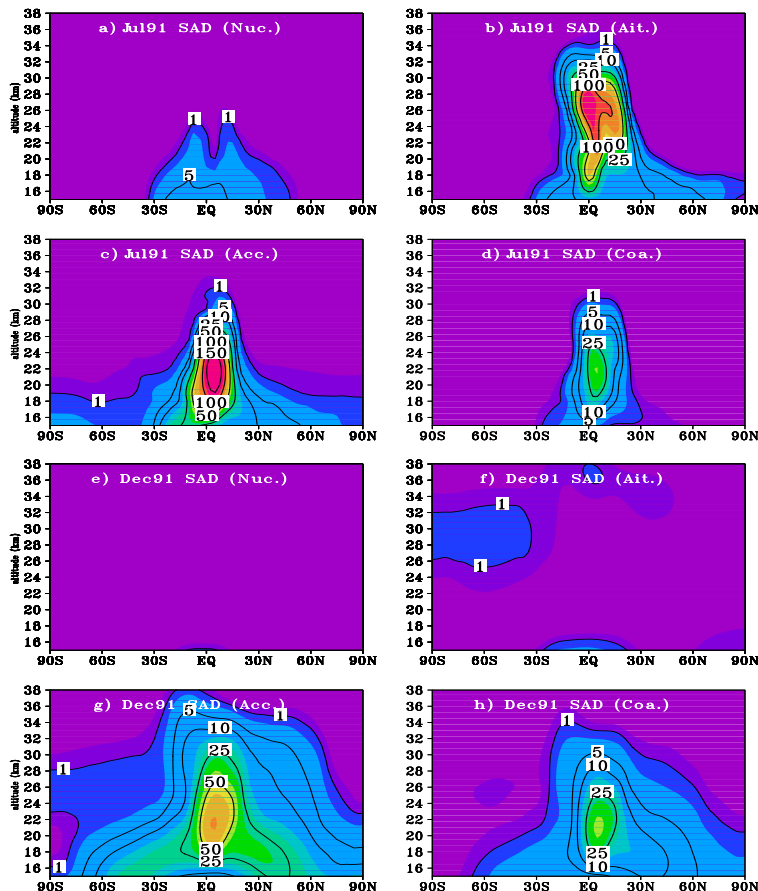


Fig. 12. Zonal mean surface area density ($\mu\text{m}^2 \text{cm}^{-3}$) for each mode against latitude and altitude for July 1991 (a, b, c, d) and December 1991 (e, f, g, h).